Authors response to reviewer #1

Dear Reviewer,

We highly appreciate your time and effort spent on reviewing our manuscript. We have prepared a new version of the manuscript with your comments taken into account. Below we include a point-by-point reply to each comment.

Comment:

"Part2.1 Ocean model in lines 28-30" Can the authors explained in more details the rescaling of the vertical coordinate?

Response:

Done.

Comment:

"Part 2.2 in lines 27, Note that the prescribed atmospheric forcing fields obtained from the PI ocean state estimate by Kurahashi-Nakamura et al., (submitted) and the corresponding isotopic fluxes are not entirely consistent and might introduce an error in our model simulation". The authors refer to unpublished results here. They should show some results that indicate what could be the error and if the use of ratio of the isotopic content indeed minimize the uncertainty.

Response:

The paper by Kurahashi-Nakamura et al., (2017) has now been published, so we added the final citation. Using the ratio of the isotopic content of precipitation and water vapor inevitably leads to isotopic fluxes that are consistent with the optimized precipitation field. To show some results, we would have to run additional simulations.

Comment:

"Part 2.3.1 in line 30". The authors compare long-term mean monthly value with GISS sample. This is indeed better than to compare with the annual mean isotope values. However, in the rest of the text it is difficult to know when the comparison is based on monthly value or annual. This is also not clear in the different figures and captions on the manuscript.

Response:

We changed both figure captions and parts of the text, to make it clearer whether we used annual mean or long-term monthly mean isotope values for the comparison.

Comment:

"Part 3.2 line21" The number of measurements for dD is rather small. According to the GISS database there is more than 1000 data points in dD. This is indeed more reduce than for the d18Osw but enough to realize a data- model comparison. Rather, the authors can mentioned that they choose to focus on the d18O and will work on the dD in the future.

Response:

We agree and rephrased the respective sentence. Due to the higher number of measurements we chose to focus on $\delta^{18}O$ to validate our model. However, since δD is now also used as a proxy in marine archives (i.e. Häggi et al. 2016) an implementation at this stage seemed reasonable.

Comment:

"Figure 3" Is it the annual or monthly value that are plotted for the model? Is it the surface data that are compared to the average 50m of the model or the data between 0 and 50 m? What could be the error associated if this is the surface data versus the average 50m?

Response:

The figure (now Fig. 4) shows the global annual mean surface (upper 50 m) $\delta^{18}O_w$ distribution of the model, while the GISS data are averaged over the upper 50 m. We rephrased the figure caption accordingly. The figure is just a first visualization of the model-data fit. For the statistical comparison (e.g. Fig. 6) we interpolated the GISS samples to the nearest tracer grid point of our model grid using inverse distance weighting. Hence, there is no error associated with the data either if it is surface data or data averaged over the upper 50 m.

Comment:

"Part 3.2 lines 3-4, the subtropical gyres are less enriched...." There is also a discrepancy for the Mediterranean Sea. What is the reason for such discrepancy in the subtropical gyres and Mediterranean region?

Response:

Based on the investigation of simulated E, P and $\delta^{18}O_w$ in P, we can conclude that the discrepancies in the subtropical gyres and the Mediterranean Sea are caused by enhanced P (having a dilutional effect on the surface water) and reduced E, whereby not enough ^{16}O is removed from the ocean surface. Even though the comparison with observed $\delta^{18}O_w$ in P is based on rather sparse data, the distribution of $\delta^{18}O_w$ in P seems to be reasonably well simulated. Further, one can assume that $\delta^{18}O_w$ in E is also slightly too enriched, but unfortunately, we cannot confirm this assumption because no observed data exists. We added these assumptions to section 4.2 and 4.3.

Comment:

"Figures 7 and 8" What is the depth used in the model (50 m?), is it annual or monthly?

Response:

The original figures showed the global annual mean $\delta^{18}O_c$ values of the surface (upper 50 m) simulated by the MITgcm. However, in response to the reviews we revised the discussion part (now section 4.4) and thus the figures (now Fig. 8 and 10) changed too. Now, we only compare modeled $\delta^{18}O_c$ values with foraminiferal calcite of plankton tow data (see last response).

Therefore, we interpolated the plankton tow data to the nearest tracer grid point of our model grid using inverse distance weighting and thus compared them to the modeled $\delta^{18}O_c$ values of the respective month and depth level of sampling.

Comment:

"Part 4.1 lines 20 to 30 and Figure 9" A zoom on the artic region would be very helpful here. The isotopic values for rivers discussed in the text could eventually be added to this figure of the artic region.

Response:

We added a zoom on the Arctic Ocean to the figure (now Fig. 13), including the approximate location of discharge of the six rivers discussed in the text. Furthermore, we included a table (Table 2) to improve the comparison between simulated river values and observed river values by Cooper et al. (2008).

Comment:

"Part 4.3: Planktonic foraminiferal d18Oc" When reading part 4.3 it seems that the main discrepancy between data and model results is because of the gametogenic calcification of foraminifera and so that paleotemperature equations derived from plankton-tow data are more appropriate to reconstruct surface water conditions that the commonly used paleotemperature equations like Shackleton (1974) or Kim and O'Neil (1997). This discussion is extremely interesting for paleoceanographic studies. Nonetheless I find that all the potential factors that can affect the d18Oc and so the data-model comparison and mismatch are not developed enough. Indeed, the temperature bias in the model (2° C or more in some regions, see figure 1) can affect significantly the d18Oc reconstruction with the model. Similarly, the bias in d18Osw could contribute significantly to this "biased towards lower values". For example, the d18Osw is 0.4‰ too depleted in the model in comparison to data in the tropics (see part 3.2) and 0.9‰ too enriched in the Arctic Ocean (see part 3.2). These biases can affect the d18Ocalcite reconstruction and comparison. Also, it seems that the shift on figure 8a is more important for tropical species than for polar species. The data-model agreement or disagreement seems different depending the oceanic region (or species considered). So I recommend to the authors to realize a data-model comparison for the d18Oc for the different species of foraminifera separately. This analyze is important not only to try to discuss the oceanic region separately but also because other factors can affect each species of foraminifera in a different way. The seasonality is one of this important factor. Although there is one sentence in the part 4.3 that mention that "seasonality could be a problem and is not considered" it would be interesting to estimate how much bias could be introduce by such inconsideration. One way to do that could be to calculate the simulated seasonal amplitude for ocean calcite d18O in the model. It could be that the "biased towards lower values" is partly or totally explained by a distortion of the foraminifera flux towards a specific season or period than the annual mean. Similarly, the effect of the vertical migration is not completely developed. The author discuss the gametogenic calcification that is indeed related to this effect of vertical migration but the different species that are grouped on Figure 8 have different depth habitats and this affect their d18Oc. They can also change their depth habitat (for example during upwelling conditions). Again a data-model comparison for each species separately and with a different mean depth habitat of calcification would be interesting.

The data on figure 8 are only presented for the first 50 m (although not clearly indicated in the text or on the Figure 8 caption). Although it will be difficult to examine the results for the very surface only (because of the grid of the model), the authors can investigate how the integration of the results for deeper water depth affect the data-model comparison.

The authors also suggest that the more enriched d18Oc values obtained with the equation of Shackleton (1974) is because this equation is based on Uvigerina spp shells that are relatively enriched in 18O. In fact, Shackleton (1974) proposed that Uvigerina peregrina is in isotopic equilibrium with seawater contrary to Cibicides. On the contrary, Bemis et al. (1998) (not cited in the discussion) suggested that Cibicides might also calcify in isotopic equilibrium and that the heavier δ18O values of Uvigerina are due to calcification at lower porewater pH. More recently, Marchitto et al., 2014 (also not cited in the discussion) investigated this difference in more details. Their results agree with Bemis et al. (1998) that Cibicidoides and Planulina appear to be closer to isotopic equilibrium (as represented by the Kim and O'Neil (1997) inorganic precipitates, which is also a matter of debate) than Uvigerina, although scatter in the measurements limits their confidence in this statement. They also recommend that Uvigerina δ18O be adjusted to the Cibicidoides scale by subtracting 0.47‰ and not 0.64‰. They were also unable to discern an impact of bottom water pH on benthic foraminiferal δ18O, but they speculate that Uvigerina's deviation from equilibrium could be explained by admixture of rapidly-precipitated non-equilibrium CaCO3 that would be subject to a pH influence. So, to my knowledge, the question as to why the δ 18O of Uvigerina and Cibicides are different remains. The question of the pH influence is also not discussed for planktonic foraminifera whereas it could also have a significant effect on the oxygen isotopic composition (Bijma et al., 1999; Zeebe 1999). This pH effect could be a primary mechanism to explain the differences between the equations (Mulitza et al., 2004). Again, the pH effect will be different with the latitudes and so it is important to discuss the species (that are associated to different oceanic regions) separately.

To resume, I like the discussion in part 4.3, this is of strong interest for paleoceanographic studies and the gametogenic calcification is a factor that certainly need to be considered. Nonetheless, the authors do not discuss in details all the factors and biases that can affect the d18Oc of their data-model comparison. For each foraminifera specie, how the bias in d18Osw in the model, the depth use in the model to generate the d18Oc signal, the seasonality and vertical migration and the pH can affect the d18Oc signal modelled and the comparison with data? At the end, if we consider all these factors and potential biases for d18Oc and the data-model comparison, can the authors really conclude that the differences between data and model is mainly linked to gametogenic calcification? If the authors cannot confirm their hypothesis in a revised version, they should also reformulate this conclusion from the abstract and conclusion part.

Response:

We agree with reviewer 1 that our discussion of foraminiferal $\delta^{18}O_c$ was too far-reaching. Indeed, many other processes (i.e. seasonal and vertical calcification, dissolution) exist that influence the composition of foraminiferal shells recorded at the sea floor, besides $\delta^{18}O_w$ and temperature. Since our model does not have an ecosystem module, many of these processes are not simulated, and we feel that our model is not the right tool to either gain information on foraminiferal ecology or on model performance. For this reason, we refrain from comparing our model results to core top $\delta^{18}O_c$ in the revised version of the paper. Plankton tow data are better constrained with respect to the time and depth of calcification. In order to demonstrate how the

combined simulation of seawater temperature and $\delta^{18}O_w$ reflects the isotopic composition of foraminiferal carbonate, we hence kept the comparison to plankton tow data.

Authors response to reviewer #2

Dear Reviewer,

We highly appreciate your time and effort spent on reviewing our manuscript. We have prepared a new version of the manuscript with your comments taken into account. Below we include a point-by-point reply to each comment.

Comment:

Page 2, line 12. Many references are missing for stable water isotopes in oceanic models: for instance, Delaygue et al, 2000, Roche et al, 2004, etc.

Response:

Done.

Comment:

Page2, Line 23. Please define "checkpoint 64w"

Response:

Done.

Comment:

Page 3 and 4, section 2.2: This section describes the methodology used for implementing the water isotopes in the MITgcm model. The simulation is forced with isotopic quantities derived from the NCAR IsoCam model, isotopic composition in precipitation and water vapor for evaporation. These quantities should be presented and discussed at least briefly in the manuscript, in order to allow further discussing the impact on oceanic model performance. Furthermore, it is also useful as the same isotopic oceanic MITgcm model could further be used with other atmospheric model forcing, it will offer the possibility to compare with the results from this study.

Response:

We included a comparison of $\delta^{18}O_w$ in P in the section 4.2 and added the global distribution as well as model-data fit as an additional figure to the manuscript (Fig. 11). Unfortunately, we do not know of any comprehensive compilation of the isotopic composition in water vapor over the ocean and thus cannot present this field.

Comment:

Page 4, Line 24: value of Ce is not specified.

Response:

C_E is specified as transfer coefficient for evaporation on page 4, line 30. For the exact definition, we added Large and Yeager (2004) as a reference, since the calculation of evaporation follows the bulk forcing approach by them.

Comment:

Page 5; line 3: the presentation of the architecture of the code should be more explicit: Apparently, gchem represent the "source and sinks" module and "ptracers" the transport module.

Response:

To clarify the purposes of the respective packages involved in the simulation of the stable water isotopes, we added an additional Table (Table 1) as an overview and rephrased the respective sentence in section 2.2.

Comment:

Page 5, line 7: Fw should be explicitly defined as Evap – precip – Runoff.

Response:

Done.

Comment:

Page 5 line 17. The freshwater flux is balanced by adjusting the precipitation field (page 3 line 14). The adjustment applied to water isotopes simulation must be described and a discussion on how it can potentially affect 180-Salinity relation is necessary.

Response:

We added the description of the calculation of the tracer specific correction factor to Appendix A and also modified Fig. A1. Due to the correction factors both the global salinity and $\delta^{18}O_w$ remains constant. Thus, any artificial drifts are prevented, which would otherwise lead to inexplicable changes in the y-intercept and slope of the $\delta^{18}O_w$-salinity relationship.

Comment:

Page 5: what is the duration of the spin-up of the simulation?

Response:

The duration of spin-up was 3000 model years (cf. section 2.1, page 3, line 20).

Comment:

Page 6 – results Section 3.1 presents model performance for temperature and salinity. Salinity anomaly should be analyzed considering the characteristics of Evaporation and Precipitation forcing fields used in this study. This will also be useful for next analyzing the water isotopes simulations.

Response:

For the presentation of the general model performance, we added zonally-averaged cross sections of temperature and salinity through the Atlantic Ocean and compared them to the GISS data. Regarding the salinity, we present precipitation and evaporation anomalies in section 4.1.

Comment:

Page 6: figure 3 : color scale is not adapted. Range (-1, 1 ‰) is too narrow to represent the more elevated values of the observations.

Response:

Done. (now Fig. 4)

Comment:

Page 6and 7 and discussion: discussion of water isotope distribution in ocean water: the discussion is too superficial. Shortcomings in water mass isotopic composition is described but the causes are never analyzed in function of model dynamical performances (AABW, NADW, AAIW formation) or surface boundary conditions (precipitation, evaporation, isotopic composition in precipitation and water vapor). A minimum more detailed analysis of the simulation is required to assess this modelling approach.

Response:

As described above, we added zonally-averaged cross sections of temperature and salinity through the Atlantic Ocean and compared them to the GISS data. Further we present precipitation and evaporation anomalies in section 4.1. The general model performance is shortly discussed in section 4.1, while the isotopic composition in precipitation is presented and discussed in section 4.2.

Comment:

Pages 9-10: discussion - the discussion of the sources of errors are mainly focuses on rivers input and sea-ice melting for the Arctic Ocean. The discussion must also consider more quantitatively the shortcomings associated to surface boundary conditions (for instance, an analysis of the realism of the isotopic composition in precipitation of the forcing has to be presented and considered, see previous comment).

Response:

We expanded the discussion on the sources of error by e.g. considering the surface boundary conditions.

Comment:

Page 11- discussion Planktonic Foraminiferal: Observation is a compilation of isotopic measurements derived on different species. The isotopic signal they register is then not obvious since the different species are living at different depth and

differently affected by the seasonal cycle. A more sophisticated approach, taking into account the characteristics of some species would be more appropriate.

Response:

We changed our comparison of modeled $\delta^{18}O_c$ with measurements by using only plankton-tow data. Since the isotopic composition of the foraminiferal shell may be altered by mechanisms such as vital effects, vertical migration and modifications after death, a comparison with living foraminifera, where the depth and month of sampling in known, seemed to be more appropriate for testing the capability of the model on reconstructing $\delta^{18}O_c$. This way different depth habitats for the different species as well as seasonal peaks should be overcome. Further, we also performed a model-data comparison for each species separately to get a better idea on sources of error for the $\delta^{18}O_c$.

Authors response to reviewer #3

Dear Reviewer,

We highly appreciate your time and effort spent on reviewing our manuscript. We have prepared a new version of the manuscript with your comments taken into account. Below we include a point-by-point reply to each comment.

Comment:

It is stated that both stable isotopes H218O and HDO have been implemented into MITgcm. However, neither simulated HDO nor Deuterium excess values are discussed anywhere in the manuscript. Even if the number of available δD in seawater observations (e.g. GISS database, Schmidt et al., 1999) or comparable model results (e.g. Xu et al., 2012) are limited, a first-order comparison would still be valuable and of high interest for on-going SWI modelling efforts within the scientific community. Alternatively, the authors might justify in more detail why they have included HDO in the MITgcm, but don't present any of the results in their paper.

Response:

For our main goal in the near future we want to use the stable water isotope package for paleoclimatic reconstructions and compare those simulations with available $\delta^{18}O_c$ of mainly benthic foraminifera. Thus, it made more sense to us to expound our model validation on the $\delta^{18}O_w$ distribution, since this is one of the main factors influencing the oxygen isotopic composition of foraminiferal shells. We slightly rephrased the beginning of part 3.2 to indicate the latter. Nevertheless, we wanted to implement HDO as a passive tracer as well to simplify the comparison with other models during investigations in the future either by the authors or other researchers who would like to use the newly developed package.

Comment:

In the manuscript, the printed equation for the equilibrium fraction factor $\alpha_{l\text{-}v}$ for HDO is wrong. In Eq. 7 of the manuscript, $\alpha_{l\text{-}v}$ is calculated as:

$\alpha_{l\text{-}v} = \exp (28.844/SST^2 * 10^3 – 76.248/SST – 5.2612*10^{-2})$

The correct equation (see Majoube, 1971, Eq. 2) reads:

$\alpha_{l\text{-}v} = \exp (28.844/SST^2 * 10^3 – 76.248/SST + 5.2612*10^{-2})$

As no HDO results are shown in this study, I cannot say if this error is simply a (double) typo in the manuscript or if the authors have indeed used a wrong HDO equilibrium factor αl-v in their simulations. In any case, this severe error has to be checked and corrected before publication.

Response:

Unfortunately, this was a typo in the manuscript. We corrected Eq. 2.

Comment:

Title: I suggest dropping the information " (checkpoint 64w) " from the title. It is sufficient mentioning the specific MITgcm model release in the Methods section.

Response:

Done.

Comment:

P2, L4/5 (=page 2, line 4/5): I recommend adding some more key references about the application of SWI in ice cores and speleothems. Just citing the studies by Johnsen et al., 2001, and Fleitmann et al., 2003, seems odd and arbitrary.

Response:

Done.

Comment:

P2, L9: correct "form" => "from"

Response:

Done.

Comment:

P2, L16: please explain in more detail why a non-linear free-surface is essential to simulate the δ-salinity relationship properly.

Response:

The salinity in the global ocean changes due to freshwater fluxes through the air-sea interface altering the ocean volume. Many ocean as well as coupled atmosphere-ocean models still use a virtual salt flux to mimic this effect. In this case, the conservation of salt requires a constant reference salinity (usually taken to be the global annual-mean surface salinity) to estimate the virtual salt flux. This way, regions that differ significantly from the reference value might be biased and the SSS cannot evolve freely. Furthermore, a restoring formulation is often employed by adding a relaxation term to the virtual salt flux to reproduce an SSS distribution that fits the observations (Huang, 1993; Roullet and Madec, 2000). This approach gives no insight in the dynamical explanation of the SSS pattern and is particularly problematic for past or future climate conditions, for which the SSS is unknown.

Using the real freshwater flux boundary conditions, the concentration and/or dilution effect is accurately simulated, whereby ocean volume changes and the SSS evolves freely. In the case of an ocean model with a free surface (as opposed to a rigid lid), a fully non-linear formulation of the free surface is required to conserve global ocean salinity.

The same reasoning applies to global $\delta^{18}O_w$ as well. Due to the real freshwater flux boundary conditions in conjunction with the non-linear free surface the salinity and $\delta^{18}O_w$ are dynamically more accurately simulated and thus the resulting $\delta^{18}O$-salinity relationship is expected to be much more realistic.

We added this information in condensed from to the introduction.

Comment:

P2, L26: the chosen vertical model resolution (15 levels) appears to be rather coarse. Please briefly discuss how this might affect the SWI simulation and model-data comparison.

Response:

Since the upper ~500 m are presented by only 4 layers in the ocean model, the thermocline might not be as pronounced as in the real ocean. Observational data that corresponds to depths within this transitional layer might reflect a different signal than resolved by the ocean model. More generally, a coarse vertical resolution makes a realistic representation of water mass boundaries and the comparison to observations (which involves vertical interpolation) more difficult. We added this information to section 4.2.

Comment:

P3, L16-18: what has been the exact criteria to determine if the PI simulation has reached "quasi steady-state"? Do SWI trends in deep ocean waters still exist at the end of the final 3000 simulation years?

Response:

We determined the quasi stead-state based on the salinity, temperature and Atlantic Meridional Overturning Circulation (AMOC). There were no critical trends visible, so that the global salinity, temperature and AMOC were approximately steady at 34.73 psu, 2.86° C and 18.24 Sv after 3000 model years, respectively. We added these criteria to the manuscript.

Regarding the stable water isotopes in the global ocean, there are no observable trends visible after the final 3000 years (for more details see response to comment to "correction factor for stable water isotope precipitation"), thus the global tracer concentration in the ocean was conserved (cf. P5, L21-22).

Comment:

P3, L25-27: why have different PI atmospheric forcing fields and isotopic fluxes been used for this simulation setup? Wouldn't it have been much more consistent to take all necessary forcing fields from the Tharammal et al., 2013, IsoCAM simulation?

Response:

Yes, it would have been, but unfortunately, we were not able to directly force the MITgcm with these fields because they led to a collapse of the overturning circulation. Therefore, we decided to use the forcing fields by Kurahashi-Nakamura et al., (2017), which were optimized to produce proper hydrographic conditions in our configuration of the MITgcm.

Comment:

P4, Eq 11: why is river runoff Ri subtracted in this equation? Conventionally, it is added to (P^i-E^i) to calculate the total isotopic surface flux.

Response:

Thank you for pointing that out. In Eq. 11 a bracket is missing. We changed Eq. 11 to:

$$F^i = -((E^i - P^i) \cdot (1 - A_{ice}) - R^i)$$

Comment:

P5, L17/18: please quantify the applied correction factor for SWI precipitation. How fast and how much would the global SWI concentration in the ocean change without this correction factor?

Response:

Without the correction factor, the stable water isotopes would not have reached a "quasi steady-state". Even after 3000 model years a continuous trend in the concentration of stable water isotopes would exist, resulting in a global $\delta^{18}O_w$ value of -0.17 ‰ (the ocean was initialized with 0 ‰). With the correction factor the stable water isotopes are steady with a global $\delta^{18}O_w$ value of -0.0003 ‰. For the quantification of the applied correction factor we modified Fig. A1 and added some additional information to the appendix A.

Comment:

P7, L20/Fig. 4b: if the authors rate the δ^{18}Ow measurements from the Okhotsk Sea as not representative for the North Pacific, these data points should be omitted in the analyses as well as Fig 4b.

Response:

The $\delta^{18}O_w$ measurements from the Okhotsk Sea are not representative for a zonally-averaged cross section of the North Pacific. To point this out we rephrased the respective sentence. However, since we show them in Fig. 4 and also use them in the model-data comparison in Fig. 6 (where we use inverse distance weighting to interpolate the GISS data to our model grid) we would like to keep them in Fig. 5b as well.

Comment:

P7, L24-26: please specify the sample number N for the different correlation calculations.

Response:

Done.

Comment:

P8, L7: omit "nicely"

Response:

Done.

Comment:

P8, L10: correct(?) “Simulated surface waters” => “Simulated calcite values”

Response:

Done.

Comment:

P9, L2: replace “is overestimated” by “is too depleted”

Response:

Done.

Comment:

P9, L2: please add “all other three Russian rivers”

Response:

Done.

Comment:

P9, 10-12: how well do the simulated annual discharge amounts agree with the observational data given in Cooper et al. (2008)? For a correct simulation of river runoff SWI into the ocean, both δ-values and total water amount are of importance.

Response:

It is difficult to determine the annual discharge amount in the MITgcm, because determining the grid cells that belong to the respective river is based on visually assigning them according to the location of the river mouth. This may lead to deviations compared to observational data. Nevertheless, when doing so, we get good agreement for the Yenisey, Lena, Yukon and Mackenzie rivers, while the Ob’ and Kolyma rivers differ substantially. But if we compare the total modeled discharge received by the Arctic basin (> 60° N) it fits quite well the observational estimate. We added this information to section 4.2 and further included a Table (Table 2) to improve the comparison.

Comment:

P10, 27-29: I don’t fully understand this argument. Please explain in some more detail the linkage between salinity restoring and SWI modelling.

Response:

As described in one of the previous responses, salinity restoring gives no insights in the dynamical explanation of the SSS pattern and is problematic for past climate conditions, where SSS is. Investigating the $\delta^{18}O$-salinity requires a free simulation of salinity and $\delta^{18}O_w$, which is possible by combining the nonlinear free surface and a real freshwater flux boundary condition. Thus, our results are an improvement compared to ocean models using virtual salt fluxes and salinity restoring, where a freely evolving salinity is not ensured.

Comment:

P11, Section 4.3: as a non-expert on planktonic foraminiferal $\delta^{18}O_c$ data, I am a bit confused by this paragraph and the given recommendations. If it is well known that core-top sediments are enriched in $\delta^{18}O_c$ due to gametogenic calcification, why have these data been compared to the simulated planktonic $\delta^{18}O_c$ values at all? And is the better agreement of sediment δ18Oc data with modelled $\delta^{18}O_c$ calculated with Shackleton's equation just by chance, then? Which procedure/equation do the authors suggest for future SWI modelling studies, if modelled $\delta^{18}O$ values shall be compared to the manifold of available planktonic $\delta^{18}O_c$ values from marine sediments?

Response:

We agree and changed our comparison of modeled $\delta^{18}O_c$ with measurements by using only plankton-tow data. Since $\delta^{18}O_c$ values measured on planktonic foraminifera from sediment cores might not reflect equilibrium with the surface ocean water due to mechanisms such as vital effects, vertical migration and modifications after death, it seemed to be more appropriate testing modeled $\delta^{18}O_c$ against living foraminifera from plankton-tows. This way any deviations due to seasonality, depth habitat, gametogenic calcification or modifications after death should be negligible.

The better agreement using the Shackleton equation was indeed due to the circumstance that it is based on the benthic foraminifera *Uvigerina spp*, which is relatively enriched in ^{18}O and produces a similar offset from equilibrium calcite as the gametogenic calcification.

The use of ecosystem models including foraminifera might ultimately provide a better understanding of the factors that determine the recording of oxygen isotopes in foraminiferal shells (Fraile et al. (2008), Lombard et al. (2009), Kretschmer et al. (2016)).

Comment:

P12, L15: "using real freshwater and isotopic flux boundary conditions" => omit "real"

Response:

We would like to keep it that way, because the term "real freshwater flux boundary conditions" is based on Huang, 1993.

Comment:

P12, L25: omit "remarkably"

Response:

Done.

Comment:

P19, Table 1: please specify in more detail how the different water masses (AAIW, NADW, AABW) have been defined and how the related $\delta^{18}O$ values have been calculated.

Response:

Done.

Comment:

P21, Fig. 2: add the unit "[psu]" to the colour bar title.

Response:

Done.

Comment:

P23, Fig. 4: please specify in more detail how the zonally averaged cross sections of $\delta^{18}O$ have been calculated.

Response:

For the calculation of the zonally-averaged cross sections we used a mask for the respective basin provided by the WOA09 and divided it into equally spaced latitudinal bands. Along those latitudinal bands a weighted zonal mean was calculated. We added those information to the figure caption of the figure (now Fig. 5).

Comment:

P23, Fig. 4: why do the plots stop at 50°S and 50°N, respectively? GISS data from higher latitudes exist and it would be valuable to compare model results and observational data in these regions of the Atlantic and Pacific, too.

Response:

Our plots in the figure (now Fig. 5) are based on the basin masks provided by the WOA09. According to the WOA09 the Atlantic and Pacific basin extend from 50° S to 60° N, thus we went along with that.

Comment:

P25, Fig. 6: do the plots show salinity and $\delta^{18}O$ values at a depth of 50m or at a depth range 0-50m? Please clarify this in the figure caption.

Response:

The figure (now Fig. 7) shows all the GISS data from a depth range of 0-50 m, either located in the tropics or mid-latitudes, while the data simulated by the MITgcm correspond to the first level of the vertical grid, thus the upper 50 m. We clarified this in the figure caption.

Stable water isotopes in the MITgcm ~~(checkpoint 64w)~~

Rike Völpel [1], André Paul[1], Annegret Krandick[1], Stefan Mulitza[1] and Michael Schulz[1]

[1]MARUM - Center for Marine Environmental Sciences and Faculty of Geosciences, University of Bremen, Bremen, Germany

Correspondence to: Rike Völpel (rvoelpel@marum.de)

Formatiert: Schriftart: (Standard) +Textkörper (Times New Roman)

Formatiert: Schriftart: (Standard) +Textkörper (Times New Roman)

Abstract.

We present the first results of the implementation of stable water isotopes in the ocean general circulation model MITgcm. The model is forced with the isotopic content of precipitation and water vapor from an atmospheric general circulation model (NCAR IsoCAM), while the fractionation during evaporation is treated explicitly in the MITgcm. Results of the equilibrium simulation under pre-industrial conditions are compared to observational data and measurements of plankton tow ~~paleoclimate records~~ (the oxygen isotopic composition of planktic foraminiferal calcite). The broad patterns and magnitude of the stable water isotopes in annual mean seawater are well captured in the model, both at the sea surface as well as in the deep ocean. However, the surface water in the Arctic Ocean is not depleted enough, due to the absence of highly depleted precipitation and snow fall. ~~too enriched river runoff~~ A model-data mismatch ~~This shortcoming in conjunction with the coarse grid resolution of the ocean model~~ is also recognizable in the isotopic composition of the seawater-salinity relationship in mid-latitudes that is mainly caused by the coarse grid resolution. Deep ~~-~~ ocean characteristics of the vertical water mass distribution in the Atlantic Ocean closely resemble observational data. The reconstructed $\delta^{18}O_c$ at the sea surface shows a good agreement with measurements. However, the model-data fit is weaker when individual species are considered and ~~D~~deviations are most likely attributable to the habitat depth of the foraminifera. ~~Apart from the systematic offset of the modeled oxygen isotopic composition of planktic foraminiferal calcite towards lower values, the comparison with proxy data shows a good agreement. We summarize that the offset is mainly caused by gametogenic calcification and a matter of choice of the applied paleotemperature equation.~~ Overall, the newly developed stable water isotope package opens wide prospects for long-term simulations in a paleoclimatic context.

1 Introduction

Stable water isotopes ($H_2{}^{16}O$, $H_2{}^{18}O$ and $HD^{16}O$ = HDO) are widely used tracers of the hydrological cycle (Craig and Gordon, 1965; Gat and Gonfiantini, 1981) and can be used to determine the origin and mixing pattern of different water masses (e.g. Jacobs et al., 1985; Khatwala et al., 1999; Meredith et al., 1999). Due to differences in their physical and chemical properties, stable water isotopes undergo fractionation processes at any phase transition within the hydrological cycle (Craig and Gordon, 1965). This leads to distinctive isotopic signatures for different freshwater fluxes, which are commonly expressed as δi (i = ^{18}O or D) with reference to the Vienna Standard Mean Ocean Water (VSMOW) standard and given as:

$$\delta i = \left(\frac{R}{R_{VSMOW}} - 1\right) \cdot 1000\ ‰\ , \quad (1)$$

where R is the ratio of the abundance of the heavier water isotope $H_2{}^{18}O$ or ~~(~~HDO~~)~~ to the abundance of the lighter isotope $H_2{}^{16}O$ and $R_{VSMOW} = 2005.2 \cdot 10^{-6}$ for $\delta^{18}O$ (Baertschi, 1976) and $155.95 \cdot 10^{-6}$ for δD (de Wit et al., 1980).

Stable water isotopes have been used as an important proxy in a wide range of climate archives, e.g. in polar ice cores which provide~~infer~~ past temperature records reflecting climatic changes over the past glacial-interglacial cycles (e.g. Dansgaard et al., 1969; Epstein et al., 1970; Johnsen et al., 1972; Johnsen et al., 2001) as well as speleothems which reveal intensity changes and variations in the amount of monsoonal rainfall (e.g. Wang et al., 2001; Fleitmann et al., 2003). ~~e.g. to infer past temperatures from ice cores (Johnsen et al., 2001) or the amount of monsoonal rainfall from speleothems (Fleitmann et al., 2003).~~ As an indirect record, stable water isotopes are preserved in carbonates ($CaCO_3$) from marine species such as planktonic and benthic foraminifers. Due to the temperature-dependent fractionation effect that occurs during the formation of $CaCO_3$, the oxygen isotopic composition of foraminiferal $CaCO_3$ ($\delta^{18}O_c$) is a function of both the ambient temperature and the isotopic composition of the seawater ($\delta^{18}O_w$) in which the calcification takes place (Emiliani, 1955). Hence, $\delta^{18}O_c$ records ~~form~~ from sediment cores provide information on water mass changes.

During the last few decades, stable water isotopes have been incorporated more extensively in general circulation models (GCMs)~~.~~, ~~f~~First ~~realizations were made~~ in atmospheric GCMs (AGCMs – e.g. Joussaume et al., 1984; Jouzel et al., 1987) and more than a decade later in oceanic GCMs (OGCMs – e.g. Schmidt, 1998; Paul et al., 1999; Delaygue et al., 2000; Wadley et al., 2002~~;~~ Roche et al., 2004; Xu et al., 2012)~~.~~, In OGCMs the focus ~~which mainly focused~~ was mainly ~~on the linear~~ relationship between $\delta^{18}O_w$ and salinity, which ~~since they~~ are affected by similar physical processes. This topic is of significant interest in paleoceanography, because it is likely that changes in advection and freshwater budgets as well as the source of precipitation may have altered this relationship (Rohling and Bigg, 1998). Using real freshwater flux boundary conditions in conjunction with the nonlinear free-surface (Huang, 1993) is essential to simulate ~~this relationship~~ it properly. Together, they ensure~~s~~ a dynamically more accurate simulation of the salinity due to the concentration and dilution effect and thus a freely evolving salinity at the sea surface.~~.~~ The Massachusetts Institute of Technology general circulation model (MITgcm) offers this very opportunity and further provides the adjoint method to perform data assimilation (Errico, 1997).

Here, we present first results of the implementation of stable water isotopes in the MITgcm, by performing an equilibrium pre-industrial (PI) simulation and comparing it to available observations and reconstructions.

2 Methods

2.1 Ocean Model

We used the MITgcm "checkpoint" 64w, which refers to a specific time and/or point within the development of the MITgcm code since it continuously undergoes updates. It~~The MITgcm ("checkpoint" 64w)~~ was configured to ~~employed,~~ solve~~ing~~ the Boussinesq, hydrostatic Navier–Stokes equations with~~and using~~ a nonlinear free-surface ~~configuration~~ (Marshall et al., 1997; Adcroft et al., 2004b). A cubed-sphere grid was used which provided a nearly uniform resolution and avoided pole singularities (Adcroft et al., 2004a). It consisted of 6 faces, each of which comprised 32 x 32 grid cells, resulting in a horizontal ~~spatial~~

Formatiert: Schriftart: (Standard) +Textkörper (Times New Roman)

Formatiert: Schriftart: (Standard) +Textkörper (Times New Roman)

resolution of approximately 2.8°. There were 15 vertical levels, ranging in thickness from 50 m at the surface to 690 m at the seafloor, giving a maximum model depth of 5200 m. Associated with the non-linear free-surface is the possible vanishing of the upper layer. To avoid this problem, the rescaled vertical coordinate z* was employed (Adcroft and Campin, 2004). This approach scales the entire vertical grid with the surface elevation and not just the surface layer (cf. Fig. 1b in Adcroft and Campin, 2004). Furthermore, the shaved cell formulation was used, which reduced the representation error of the bathymetry (Adcroft et al., 1997). The model was coupled to a dynamic-thermodynamic sea ice model with a viscous-plastic rheology (Losch et al., 2010).

Isopycnal diffusion and eddy-induced mixing was parameterized with the GM/Redi scheme (Redi, 1982; Gent and McWilliams, 1990). Background vertical diffusivity for tracers was uniform at $3 \cdot 10^{-5}$ [m^2 s^{-1}], and for the equation of state the polynomial approximation of Jackett and McDougall (1995) was used. Advection of tracers was computed using third-order advection with direct space-time treatment (Hundsdorfer and Trompert, 1994).

Atmospheric forcing (air temperature, specific humidity, zonal and meridional wind velocity, wind speed, (snow-) precipitation, incoming shortwave and longwave radiation as well as river runoff – 12 ~~months~~ climatological monthly means) was obtained from the PI ocean state estimate by Kurahashi-Nakamura et al., (2017~~submitted~~), which was based on the protocol of the Coordinated Ocean-ice Reference Experiments (COREs) project (Griffies et al., 2009). They optimized the forcing fields to reconstruct tracer distributions that were consistent with observations. Air-sea fluxes were internally computed in the model following the bulk forcing approach by Large and Yeager (2004). Furthermore, we globally balanced the freshwater flux by annually adjusting the precipitation field (Appendix A).

Our simulation was initialized with present-day salinity and temperature distributions (Levitus et al., 1994 and Levitus and Boyer 1994, respectively) and spun up from the state of rest. We used asynchronous time stepping to accelerate computation with a time step of 1 day for the tracer equations and 20 min. for the momentum equations.

~~Furthermore, we globally balanced the freshwater flux by annually adjusting the precipitation field (Appendix A).~~ We compiled the code using the GNU Fortran compiler gfortran version 5.3.0 and performed the simulation on 6 cores of a processor of type Intel Xeon E5-2630 v3. The simulation was integrated for 3000 years (1000 model years took ~ 7.5 CPU hours) to reach a quasi-steady state (the global salinity, temperature and Atlantic Meridional Overturning Circulation were approximately steady at 34.73 psu, 2.86° C and 18.24 Sv (1 Sv = 10^6 m^3 s^{-1}) respectively), continued for a further 3000 years with stable water isotopes as passive tracers. For analysis, the average of the last 100 years was used.

2.2 Implementation of water isotopes

We implemented the stable water isotopes $H_2{}^{16}O$, $H_2{}^{18}O$ and HDO as conservative, passive tracers in the ocean component of the MITgcm (wiso package). Isotopic variations at the sea surface were driven by evaporation (E), precipitation (P) and river runoff (R), while advection, diffusion and convection affected the distribution in the interior of the ocean. Monthly climatological means of the isotopic content of precipitation and water vapor were available from the National Center for

Atmospheric Research Community Atmosphere Model including a water isotope scheme (NCAR IsoCAM – Tharammal et al., 2013). Note that ~~–~~the prescribed atmospheric forcing fields obtained from the PI ocean state estimate by Kurahashi-Nakamura et al., (2017~~submitted~~) and the corresponding isotopic fluxes are not entirely consistent and might introduce an error in our model simulation. However, to minimize the uncertainty we only took the ratio of the isotopic content of precipitation and water vapor and applied it to the corresponding atmospheric forcing fields. The isotopic composition of river runoff affects the isotopic composition of ocean water ($\delta^{18}O_w$ and δD_w) particularly in coastal regions. Since there was no land model in the MITgcm to calculate the amount and isotopic composition of continental runoff, we assumed that it equals the isotopic composition of the local precipitation at the river mouth and again applied it to the runoff forcing field.

Fractionation during evaporation, taking both equilibrium effects and kinetic effects into account, was treated explicitly in the MITgcm. The formulation for the isotopic composition of evaporation E^i [mol m^{-2} s^{-1}] is

$$E^i = \Gamma^i (q^i - q_s^i), \quad (2)$$

Here, q^{i*} is the specific humidity [kg kg^{-1}] multiplied by the isotopic ratio derived from the NCAR IsoCAM and

$$q_s^{i*} = q_s \frac{J^{i*}}{\alpha_{l-v}} \quad (3)$$

is the tracer specific humidity [kg kg^{-1}] in thermodynamic equilibrium with the liquid at the ocean surface (Merlivat and Jouzel, 1979), ~~w~~While

$$q_s = \frac{0.98}{\rho_{air}} q_{sat} \quad (4)$$

is the local sea surface humidity [kg ~~/~~kg^{-1}] with q_{sat} being the saturation specific humidity [kg m^{-3}] and ρ_{air} being the atmospheric density [kg m^{-3}],

$$J^i = \frac{c(i) \cdot M(i)}{c(H_2{}^{16}O) \cdot M(H_2{}^{16}O)} \quad (5)$$

is the local sea surface mass ratio with c being the concentration [mol m^{-3}] and M the molar mass [g mol^{-1}] of the respective stable water isotope. The equilibrium fractionation factor $\alpha_{l\text{-}v}$ between liquid water and water vapor has been found empirically as a function of temperature and was given by Majoube (1971):

$$\alpha_{l-v}^{\delta^{18}O} = e^{\frac{1.137}{SST^2} \cdot 10^3 - \frac{0.4156}{SST} - 2.0667 \cdot 10^{-3}} \quad (6)$$

$$\alpha_{l-v}^{\delta D} = e^{\frac{28.844}{SST^2} \cdot 10^3 - \frac{76.248}{SST} + 5.2612 \cdot 10^{-2}} \quad (7)$$

with SST being the sea surface temperature [K].

Due to different molecular diffusivities of the isotopes, kinetic fractionation occurs. The kinetic fractionation factor K depends on wind speed U [m s^{-1}] through the roughness of the air-sea interface (Merlivat and Jouzel 1979; Jouzel et al., 1987):

$$K_{H_2^{18}O} = \begin{cases} 0.006, & if\ U < 7\ m\ s^{-1} \\ 0.000285 \cdot U + 0.00082, & if\ U \geq 7\ m\ s^{-1} \end{cases} \quad (8)$$

$$K_{HDO} = \begin{cases} 0.00528, & if\ U < 7\ m\ s^{-1} \\ 0.0002508 \cdot U + 0.0007216, & if\ U \geq 7\ m\ s^{-1} \end{cases} \quad (9)$$

Formatiert: Schriftart: (Standard) +Textkörper (Times New Roman)

Formatiert: Schriftart: (Standard) +Textkörper (Times New Roman)

Formatiert: Schriftart: (Standard) +Textkörper (Times New Roman)

Formatiert: Schriftart: (Standard) +Textkörper (Times New Roman)

Formatiert: Schriftart: (Standard) +Textkörper (Times New Roman)

Formatiert: Schriftart: (Standard) +Textkörper (Times New Roman)

Formatiert: Schriftart: (Standard) +Textkörper (Times New Roman)

Formatiert: Schriftart: (Standard) +Textkörper (Times New Roman)

The kinetic fractionation factor was used to calculate the isotopic profile coefficient Γ^i following:

$$\Gamma^{i*} = \rho C_E U(1-K) \quad (10)$$

where ρ is the air density and C_E is the transfer coefficient for evaporation as described in Large and Yeager (2004). Fractionation during the formation of sea ice was neglected, because it is very small compared to other fractionation processes and thus only leads to minor effects on $\delta^{18}O_w$ and δD_w (Craig and Gordon, 1965). Due to the absence of isotopes in the sea ice we approximated the isotopic surface flux F^i [mol m^{-3} s^{-1}] by:

$$F^i = -((E^i - P^i) \cdot (1 - A_{ice}) - R^i) \quad (11)$$

with A_{ice} being the ice-covered area fraction. Based on this approximation, there was no isotopic surface flux in areas covered by sea ice unless they were influenced by river runoff. Within the MITgcm, processes that affected the stable water isotopes were taken care of by the "gchem" and "ptracers" packages (Table 1). While the "gchem" package acted as an interface between the ptracers and wiso package and added F^i to the passive tracer surface tendency $gPtr^i$ [mol m^{-3} s^{-1}]

$$gPtr^i = gPtr^i + F^i \quad (12)$$

the "ptracers" package mainly accounted for the transport of the isotopes by advectingon and diffusing themon of the isotopes. Furthermore, due to the freshwater flux that effectively changed the water column height, an additional tracer flux F_w^i [mol m^{-2} s^{-1}] associated with this input/output of freshwater ($E - P - R$ ~~F_w~~ [kg m^{-2} s^{-1}]) was calculated following

$$F_w^i = (E - P - R)\,\text{~~}F_w\text{~~} \cdot c_i \cdot x \quad (13)$$

with x being an units conversion factor. F_w^i was then additionally added to the tracer surface tendency within the "ptracers" package

$$gPtr^i = gPtr^i + F_w^i \cdot \frac{1}{z} \quad (14)$$

with z [m] being the surface grid cell thickness.

In the MITgcm, the stable water isotopes were not treated as ratios, but as individual concentrations. Therefore, we initialized the ocean with homogenous concentrations of $H_2{}^{16}O$, $H_2{}^{18}O$ and HDO matching present-day $\delta^{18}O_w$ and δD_w values of 0‰ with reference to the VSMOW. The ratios were calculated during the analysis of the results.

Furthermore, similar to the freshwater flux, a correction factor for the tracer specific precipitation was applied, whereby the respective global tracer concentration in the ocean was conserved (cf. Appendix A).

2.3 Observational data

2.3.1 $\delta^{18}O_w$ data

The Goddard Institute for Space Studies (GISS) Global Seawater Oxygen-18 Database v1.21 comprises over 26,000 seawater $\delta^{18}O$ values collected since about 1950 (Schmidt et al., 1999) and therefore offers an opportunity to evaluate~~validate~~ the modeled oceanic $\delta^{18}O$ values.

Formatiert: Schriftart: (Standard) +Textkörper (Times New Roman)

Formatiert: Schriftart: (Standard) +Textkörper (Times New Roman)

Formatiert: Schriftart: (Standard) +Textkörper (Times New Roman)

Formatiert: Schriftart: (Standard) +Textkörper (Times New Roman)

Formatiert: Schriftart: (Standard) +Textkörper (Times New Roman)

Formatiert: Schriftart: (Standard) +Textkörper (Times New Roman)

Formatiert: Schriftart: (Standard) +Textkörper (Times New Roman)

Formatiert: Schriftart: (Standard) +Textkörper (Times New Roman)

For comparison, we interpolated the GISS samples to the nearest tracer grid point of our model grid using inverse distance weighting. We excluded any data point with applied correction, from enclosed lagoons, representing estuarine or river data from near the coast or heavily influenced by meltwater, which means that we rejected all data points flagged as G, H, I, J, L and X in the GISS database (see Schmidt et al., 1999 for details – 23,232 data points remained). We could not expect our model to reproduce such conditions, based on our relatively coarse grid resolution.

Since the GISS data usually represent samples taken at a certain time during the year, we did not compare them to simulated annual mean isotope values. Instead, we used a long-term ~~mean~~ monthly mean value of the specific month, when the GISS sample was measured.

2.3.2 $\delta^{18}O_c$ data

Mulitza et al. (2003) compiled a number of $\delta^{18}O_c$ values measured on planktonic foraminifera from plankton tows (including data from Duplessy et al., 1981, Kahn and Williams 1981, Ganssen 1983, Bauch et al., 1997 and Peeters and Brummer~~et al.~~, 2002). They limited their compilation on the four species *Globigerinoides ruber* white (*G. ruber* (w)), *Globigerina bulloides* (*G. bulloides*), *Neogloboquadrina pachyderma* sinistral (*N. pachyderma* (s)) and *Globigerinoides sacculifer* (*G. sacculifer*), since these species are very abundant, cover a broad geographical and temporal range and belong to the shallowest-dwelling planktonic foraminifera. We extended this data set with available *in situ* $\delta^{18}O_c$ data from Kohfeld and Fairbanks (1996), Moos (2000), Stangeew (2001), Volkmann and Mensch (2001), Mortyn and Charles (2003), Keigwin et al. (2005), Wilke et al. (2009) and Rippert et al. (2016). By using inverse distance weighting, we interpolated the $\delta^{18}O_c$ data to the nearest tracer grid point of the MITgcm grid (analogous to the GISS data) and compared them to the simulated long-term monthly mean $\delta^{18}O_c$ values of the respective month of sampling. We used the paleotemperature equation from Mulitza et al. (2004)

$$T\,[°C] = 14.32 - 4.28 \cdot (\delta^{18}O_c - \delta^{18}O_w) + 0.07 \cdot (\delta^{18}O_c - \delta^{18}O_w)^2 \quad (15)$$

to determine the dependency between ~~Waelbroeck et al. (2005) provide a global compilation of $\delta^{18}O_c$ that has been assembled within the Multiproxy Approach for the Reconstruction of the Glacial Ocean surface (MARGO) project. It contains over 2100 core-top and Late Holocene data from planktic foraminifera, mainly measured in *Globigerinoides ruber pink* and *white*, *Globigerina bulloides*, *Neogloboquadrina pachyderma* sinistral and dextral and *Globigerinoides sacculifer* and was used for comparison. T~~the ~~isotopic composition of calcite~~ ($\delta^{18}O_c$)~~, is linked to~~ the temperature T during calcification and the $\delta^{18}O_w$. ~~We used the paleotemperature equation from Mulitza et al. (2004)~~

~~$T\,[°C] = 14.32 - 4.28 \cdot (\delta^{18}O_c - \delta^{18}O_w) + 0.07 \cdot (\delta^{18}O_c - \delta^{18}O_w)^2$ (15)~~

~~to determine this dependency.~~ Since water samples are reported relative to the VSMOW standard and carbonate samples relative to the Vienna PeeDee Belemnite (VPDB) standard, the $\delta^{18}O_w$ values need to be converted by subtracting -0.27 ‰ (Hut, 1987).

Formatiert: Schriftart: (Standard) +Textkörper (Times New Roman)

Formatiert: Schriftart: (Standard) +Textkörper (Times New Roman)

3 Results

3.1 General model performance – temperature and salinity distribution ~~Temperature and salinity distribution at the sea surface~~

We compare the simulated annual mean SST and sea surface salinity (SSS, upper 50 m) to the annual mean (averaged over the upper 50 m and interpolated to the cubed sphere grid) temperature (Fig. 1a, b) and salinity (Fig. 2a, b) of the World Ocean Atlas 2013 (WOA13 – Locarnini et al.~~,~~ (2013), Zweng et al. (2013), respectively~~, respectively (Fig. 1a, b and 2a, b)~~. In most regions of the W~~w~~orld O~~o~~cean, SST differences are around 1 °C or even less (root mean square error (RMSE) = 1.18 °C) and therefore in good agreement with the data. Larger differences are mainly located in regions of coastal and equatorial upwelling, in the Gulf Stream and around Indonesia.

A different picture emerges for the SSS anomaly. While most parts of the surface ocean are slightly too fresh, especially the Mediterranean Sea, Bay of Bengal, Hudson Bay and north of Iceland, both the Arctic Ocean and the east coast of North America are too salty. Nevertheless, we obtain a RMSE of 0.45 psu without using any salinity restoring.

This good agreement also continues in the deeper parts of the Atlantic Ocean. Calculated weighted zonal means of the simulated annual mean temperature and salinity in the Atlantic Ocean correspond well with the observations (Fig. 3a and b respectively; temperature and salinity provided by the GISS data – Schmidt et al., 1999). The simulated annual mean temperature gradually decreases with depth, as do the observational data. It is also recognizable that the boundary towards water masses colder than 4 °C appears slightly shallower in the southern than in the northern part of the Atlantic Ocean. Coldest temperatures occur in the deep southern Atlantic Ocean, both in the simulated as well as observational data. Interpolating the observational data to the nearest tracer grid point and comparing it to the simulated long-term ~~mean~~ monthly mean values of the respective month of sampling (as described in section 2.3.1 for the GISS data), further underlines the agreement between simulated and observed values (Fig. 3c – r^2 = 0.93, RMSE = 2.1 °C, n = 660). The zonally-averaged cross section of the simulated annual mean salinity clearly reveals the occurrence of different water masses. While most parts of the Atlantic Ocean are filled by the North Atlantic Deep Water (NADW) coming from the north with a salinity value of around 34.9 psu (reaching a water depth of ~ 3500 m), the deepest parts of the Atlantic Ocean basin are occupied by less saline water (~ 34.7 psu) of the Antarctic Bottom Water (AABW) flowing from the south. The Antarctic Intermediate Water (AAIW) is the freshest water mass (~ 34.6 psu) and can be traced as a tongue, spreading from the south towards the north at a water depth of 1000 m. The ~~M~~most ~~pronounced~~ saline water appears in the upper water column of the northern tropics (~ 30° N). This structure is also reflected in the observational data, however both NADW and AAIW seem to be slightly fresher. Performing a model-data comparison for salinity, as outlined above for temperature, shows a good fit (Fig. 3d – r^2 = 0.61, RMSE = 0.6 psu, n = 691) in general, but a few points are clearly located above the 1:1 line. These data points correspond to simulated annual mean salinity values in the upper water column near the North American coast, one of the regions with the highest~~most~~ positive SSS anomalies (Fig. 2a) and will be discussed shortly in section 4.1.

3.2 Stable water isotope distribution in ocean water

Even though measurements of δD exist, they are not as widespread as $\delta^{18}O$. Furthermore, the stable water isotope package will be used mainly for paleoclimatic reconstructions in conjunction with ~~proxy data mainly~~ $\delta^{18}O_c$ data from~~of~~ benthic foraminiferal shells. Hence, we chose to focus on the comparison for $\delta^{18}O$ to validate our simulation.~~In the following, we will only focus on the comparison for $\delta^{18}O$, since the number of measurements for δD is rather small.~~

The surface (upper 50 m) distribution of annual $\delta^{18}O_w$ simulated by the MITgcm gradually decreases from the mid-latitudes to high latitudes (Fig. 4~~3~~a, b). Highest values of about 1 ‰ occur in the subtropical gyre of the Atlantic Ocean, which are slightly higher than in the Pacific Ocean, reflecting the net freshwater transport by the trade winds. The Mediterranean Sea and Red Sea are regions of net evaporation and therefore contain $\delta^{18}O_w$ values of similar magnitude. The most depleted surface water is simulated in the high latitudes, showing values of -0.5 ‰ in the Southern Ocean and -1 ‰ in the Arctic Ocean. These depleted values result from negative $\delta^{18}O_w$ values in precipitation in combination with river/glacial runoff. Similarly, depleted values occur in surface waters around Indonesia.

The large~~-~~-scale pattern~~s~~ and latitudinal gradients of simulated annual mean $\delta^{18}O_w$ values match fairly well the observations. For example, the model captures the contrast between high and low latitudes and the Atlantic and Pacific Ocean. However, some notable discrepancies are recognizable when comparing the absolute range of $\delta^{18}O_w$ at the surface. ~~The subtropical gyres are less enriched I~~in the MITgcm, the subtropical gyres are less enriched than in the observations (annual mean value of 0.6 ‰ as compared to 1.0 ‰, respectively). The same holds true for ~~as well as~~ the Mediterranean Sea.~~,~~ For the Arctic Ocean ~~while~~ simulated $\delta^{18}O_w$ values ~~in the Arctic Ocean~~ are not as depleted as in the observational data (annual mean value -0.6 ‰ as compared to -1.5 ‰, respectively). Especially near large river estuaries, the model-data mismatch is large.

A clear distinction between different water masses based on the annual mean isotopic composition of sea water is recognizable in our simulation, both for the Atlantic Ocean and the Pacific Ocean (Fig. 5~~4~~a and 5~~4~~b respectively). In our model, the ~~North Atlantic Deep Water (~~ NADW~~)~~ in the Atlantic Ocean reaches down to approximately 3500 m depth and is rather enriched in $H_2{}^{18}O$, resulting in an annual mean $\delta^{18}O_w$ content of around 0.11 ‰ (cf. Table 3~~2~~1). Most enriched $\delta^{18}O_w$ values (~ 0.6 ‰) occur in the upper water column of the tropics (20° - 30~~-~~° S and N). The NADW encounters the ~~Antarctic Intermediate Water (~~AAIW~~)~~ coming from the south at a water depth of approximately 1000 m. The latter is more depleted with an annual mean $\delta^{18}O_w$ value of around 0 ‰. The deepest parts of the Atlantic Ocean are characterized by negative annual mean $\delta^{18}O_w$ values of approximately -0.11 ‰ derived from ~~the~~ ~~Antarctic Bottom Water (~~AABW~~)~~ mixed with NADW. This water mass structure is ~~also recognizable~~ in good agreement with~~in~~ the observational data~~, and therefore in good agreement.~~ However, the NADW is not enriched enough compared to the observational data (0.21 ‰), whereby the deepest parts of the Atlantic Ocean reveal too depleted $\delta^{18}O_w$ values. For the Pacific Ocean (Fig. 5~~4~~b) the vertical structure is even more homogenous~~ly stratified~~. Enriched waters (~0.1 ‰) occur in the upper water column down to approximately 1000 m. Deeper parts of the Pacific are filled with depleted water of around -0.1 ‰. Compared to the observational data, the vertical and latitudinal gradients are in

agreement. The large number of negative $\delta^{18}O_w$ measurements at 50° N is obtained from the Okhotsk Sea and thus is not representative for a zonally-averaged cross section of the North Pacific.

To take a closer look at the model-data fit, we interpolated the GISS data to the nearest tracer grid point and compared it to the simulated long-term ~~mean~~ monthly mean value of the respective month of sampling (see section 2.3.1). The separation of the model-data comparison into different ocean basins (Atlantic Ocean - Fig. 6~~5~~a, Pacific Ocean - Fig. 6~~5~~b, Arctic Ocean - Fig. 6~~5~~c and Indian Ocean - Fig. 6~~5~~d) points to deviations that mainly occur in higher latitudes. The correlation and RMSE is quite diverse, showing strong correlation for the Indian (r^2 = 0.77, RMSE = 0.19 ‰, n = 593) and Pacific Ocean (r^2 = 0.74, RMSE = 0.32 ‰, n = 743), medium correlation for the Atlantic Ocean (r^2 = 0.37, RMSE = 0.79 ‰, n = 756) and no correlation for the Arctic Ocean (r^2 = 0.05, RMSE = 1.18 ‰, n = 1048). Overall, depleted $\delta^{18}O_w$ values are not very well simulated in the MITgcm, which is particularly recognizable in the Arctic, a region highly influenced by negative $\delta^{18}O_w$ values from precipitation, snow fall and river runoff (Yi et al., 2012).

3.3 Relationship between ~~S~~stable water isotopes and salinity ~~relation~~

Formatiert: Schriftart: (Standard) +Textkörper (Times New Roman)

Formatiert: Schriftart: (Standard) +Textkörper (Times New Roman)

Similar physical processes determine the salinity and $\delta^{18}O_w$ distribution at the ocean surface. ~~Thus~~Thus, locally a linear relationship between those two quantities can be expected. Therefore, we compared the modeled $\delta^{18}O_w$-salinity relationship with the observed one by taking the closest long-term monthly mean tracer grid value of salinity and $\delta^{18}O_w$ to the GISS ~~datapoints~~data points of the respective month of sampling. Restricting the comparison to the upper 50 m and ~~Restricting~~ the salinity range to 28 – 38 psu in order to reflect open ocean conditions, the general features of the latter relationship are well captured in our model (Fig. 7~~6~~).

The modeled $\delta^{18}O_w$-salinity relationship in the tropics (25° S – 25° N) agrees quite well with the observed one (Fig. 7~~6~~a). Here, we find a simulated slope of 0.15 ‰ psu^{-1}, while the observed one is 0.22 ‰ psu^{-1}. A steeper slope is visible in the mid-latitudes (25° S/N – 60° S/N) for both the simulated and observed relationship (Fig. 7~~6~~b). However, the agreement between those two slopes is smaller than in the tropics ~~slightly decreases~~, with a simulated slope of 0.28 ‰ psu^{-1} and an observed slope of 0.49 ‰ psu^{-1}. Further, it underlines that we do not simulate salinity and $\delta^{18}O_w$ values as low as represented in the GISS data.

3.4 $\delta^{18}O_c$ distribution

The annual mean simulated $\delta^{18}O_c$ distribution at the surface (upper 50 m) increases from the tropical regions (~ 3‰) to high latitudes (~ 3.5 ‰), ~~nicely~~ reflecting the dependency on both $\delta^{18}O_w$ and temperature (Fig. 8~~7~~). Most depleted $\delta^{18}O_c$ values develop~~occur~~ in the Bay of Bengal and around Indonesia (< 3.5 ‰), while the transition towards positive $\delta^{18}O_c$ values occurs~~emerge~~ from 40° S/N upwards. Even though the plankton tow data are rather sparsely distributed in the global ocean, a latitudinal increase in $\delta^{18}O_c$ is also recognizable. ~~Even though most of the observational data is located in the North Atlantic, a latitudinal increase in $\delta^{18}O_c$ is recognizable.~~ Thus, the simulated large-scale pattern and latitudinal gradient match fairly well the measurements. Nevertheless, some model-data mismatch occurs. Simulated ~~surface waters~~annual mean calcite values in the tropics seem to be slightly too low (e.g. northeast of the Amazon delta), while regions in the North Atlantic and Arctic

Ocean are slightly enriched compared to the observations. The influence of the ~~model is characterized by a~~ seasonal cycle ~~which~~ on~~influences~~ the $\delta^{18}O_c$ distribution~~differently~~ depend~~sing~~ on latitude (Fig. 9). The ~~L~~largest seasonal effects occur in the northern mid-latitudes (30° - 60° N) with values of up to 3 ‰, whereas a weak or almost no seasonal effect appears in low and high latitudes. Thus, when performing a model-data comparison, ~~to exclude mismatches due to seasonality the simulated long-term monthly mean value of~~ the respective month of plankton tow sampling must be~~is~~ considered.~~, when performing a model-data comparison.~~ Figure 10a and b include not just the surface data but plankton tows taken in deeper parts of the ocean. The comparison reveals a good match (r^2 = 0.88, RMSE = 0.83 ‰, n = 183). Data points that are not located along the 1:1 line but rather above, belong either to the deeper water columns of the model (Fig. 10b) within the tropics (Fig. 10a) or, as mentioned above, to the upper water column (Fig. 10b) in high latitudes (Fig. 10a).

~~around Indonesia are too depleted as well as along coastal upwelling regions and in the Mediterranean Sea. Furthermore, regions in the North Atlantic, which are influenced by the Gulf Stream, are not sufficiently enriched compared to the observations. Overall, the simulated $\delta^{18}O_c$ distribution at the surface slightly tends to be too low~~ tends to be slightly too low~~. This becomes even clearer when performing a model-data comparison (Fig. 8a) by interpolating the $\delta^{18}O_c$ data to the nearest tracer grid point (analogously to the GISS data). Most of the data points plot below the 1:1 line. The cause for this bias is a matter of investigation and will be discussed in section 4.3. Nevertheless, we get a strong correlation with r^2 = 0.90 and RMSE = 1.01 ‰.~~

4 Discussion

4.1 Model performance

Before we discuss the $\delta^{18}O_w$ distribution in the MITgcm, the general model performance will be shortly assessed, because an accurate presentation of the ocean circulation is essential for a reasonable simulation of stable water isotopes. Therefore, we investigate the temperature and salinity distribution, because these two quantities determine the density and thus one of the main factors influencing the vertical movement of ocean waters. The results for the simulated annual mean temperature and salinity are quite promising. Large biases at the sea surface occur in the North Atlantic, both for the SST and SSS. These biases are quite common in ocean models, especially with a low resolution, since the proper simulation of the structure, pathways and extensions of western boundary currents are difficult to achieve (cf. Gri~~i~~ffies et al., 2009). Here, the Gulf Stream remains attached to the coast far to north and due to the coarse grid resolution subpolar surface water displaces the North Atlantic Current resulting in SST and SSS biases. Regarding the SST, warm biases also occur in the upwelling regions along the west coasts of Africa and America (intruding far into the open ocean basin), which are~~is~~ mainly driven by the poorly resolved coastal upwelling process. ~~in conjunction with the coarse resolution of the grid, but may also be triggered from errors in the near coastal wind directions.~~ In terms of SSS biases, surface boundary conditions like *P* and *E* should be considered. In general, the large-scale patterns for *P* and *E* are accurately presented (not shown here). The prescribed precipitation field *P* clearly~~nicely~~ depicts the intertropical convergence zones (ITCZ) in the Atlantic and Pacific Ocean~~s~~. Further, extremely dry ocean regions

in the subtropics that are associated with high pressure zones are visible. The simulated evaporation field ~~Global~~ *E* is mainly zonally oriented, with increased values occurring in subtropical areas and decreased values along the equator and high latitudes. This zonal pattern is interrupted in regions of western boundary currents, where *E* is enhanced along the pathways. For a more precise estimate, we calculated annual anomalies for *P* and *E* (Fig. 11a and b, respectively) using data from rain gauge stations from the Global Precipitation Climatology Project (GPCP – Huffman et al., 1997) and the latent heat flux (converted to *E* by dividing it with the constant latent heat of evaporation ($2.5 \cdot 10^6$ [J kg^{-1}] – Hartmann, 1994)) from the National Oceanography Centre (NOC) Version 2.0 Surface Flux and Meteorological Dataset (Berry et al., 2009). Unfortunately, no data exists for *E* in high latitudes, whereby no model-data comparison can be carried out in these regions. Since *E*, among others, depends on the SST, a similar picture for the anomaly should emerge. Indeed, regions with warmer (colder) SST simulated by the MITgcm also experience elevated (reduced) *E* values. The precipitation however, is too small in the North Atlantic, the Bay of Bengal, the equatorial Atlantic ~~equator~~ and along 60° S, while too large mainly in the tropics (especially in the Pacific) and high latitudes. Regarding the SSS, the bias in the North Atlantic appears to be~~described above is exemplary for the coupling between SST and SSS through the evaporative flux. Here we assume that the SSS bias is~~ caused by an interaction between the coarse grid resolution and a bias in the evaporation~~inappropriate *E*~~. Besides the Mediterranean Sea, where enhanced *P* and reduced *E* lead to a fresh bias, there is no other apparent correlation between *P*, *E* and SSS anomalies. ~~Compared to other ocean simulations, our results are reasonable.~~ With a RMSE of 1.18 °C and 0.45 psu, respectively, our SST and SSS results are comparable to Danabasoglu et al. (2012), who reported a RMSE of 0.58 °C and 0.41 psu for the POP2 ocean component of the Community Climate System Model 4 (CCSM4) using a weak salinity restoring, and Griffies et al. (2011), who got a RMSE of 1.3 °C and 0.77 psu with the Geophysical Fluid Dynamics Laboratory Climate Model version 3.

Likewise, the comparison with observed data for the deep Atlantic Ocean basin is good. The main water masses AAIW, NADW and AABW can be detected. Core properties of the water masses (AAIW: salinity = ~ 34.6 psu, temperature = ~ 5 °C; NADW: salinity = ~ 34.9 psu, temperature = ~ 3 °C; AABW: salinity = ~ 34.7 psu, temperature = ~ 0 °C; visual estimation based on Fig. 3) fit reasonably well the temperature and salinity ranges reported by Emery and Meincke (1986 – Fig. 14, rectangles). But both, NADW and AABW might be slightly too salty, while the AABW ~~also~~ seems to be too cold~~er~~. To maintain a realistic ocean climate, not just the water mass structure is of importance but also the circulation ~~transport~~ strength. The maximum meridional transport at 48° N simulated in the MITgcm is 17.8 Sv, consistent with 16 ± 2 Sv reported by Ganachaud (2003) and Lumpkin et al. (2008).

Thus, we find~~claim~~ that the general model performance is reasonable and comparable to both observations and other climate simulations.

4.2~~1~~ Sources of error for $\delta^{18}O_w$

Results of the $\delta^{18}O_w$ distribution at the sea surface showed relatively large mismatches between modeled and observed data in the Arctic Ocean. As indicated by Eq. 11, there is no isotopic surface flux in areas that are covered by sea ice unless they are

influenced by river runoff. Since parts of the Arctic Ocean are covered by sea ice all year round and others are seasonally influenced (not shown here), these areas do not experience any isotopic surface flux during most of the year. In this way, the impact of precipitation and snow fall that is highly depleted is neglected, which could explain too high $\delta^{18}O_w$ values in the Arctic Ocean.

The spatial ~~Both, iIn general, the accurate~~ distribution of $\delta^{18}O_w$ in *P* is also a matter of debate. The Global Network of Isotopes in Precipitation (GNIP – IAEA/WMO, 2010) provides a database with $\delta^{18}O_w$ in *P* at more than 950 stations all around the globe. For the comparison with modeled annual $\delta^{18}O_w$ in *P* only data with continuous sampling for a minimum of 5 years has been considered, resulting in 127 data points. Unfortunately, most of the data is continental, whereby a significant conclusion for the $\delta^{18}O_w$ in *P* over the ocean is difficult. Nevertheless, all the main characteristics in $\delta^{18}O_w$ in *P* can be identified (Fig. 12a). Due to the temperature effect on the fractionation during condensation (Dansgaard, 1964), $\delta^{18}O_w$ in *P* decreases from mid- to high latitudes. While most ~~annual~~ enriched values occur in the regions of trade winds with slightly more depleted values along the ITCZ, the strongest depletion can be found over the polar ice sheets. For a more straightforward statement, we performed a model-data comparison (Fig. 12b) by interpolating the GNIP data to the closest tracer grid point of the MITgcm, revealing a good agreement between modeled and measured data ($r^2 = 0.72$, RMSE = 2.4 ‰, n = 91). Linking these results to the large~~st~~ $\delta^{18}O_w$ mismatches that emerged in the Arctic Ocean, subtropical gyres and the Mediterranean Sea~~,~~ let us conclude~~assume~~ that the decreased $\delta^{18}O_w$ values at the ocean surface in the latter~~st~~ two ~~mentioned~~ regions~~,~~ are caused by an interaction of *P*, *E* and $\delta^{18}O_w$ in *E*. Enhanced *P* in the MITgcm has a dilutional effect on the water, while due to reduced *E* not enough ^{16}O is removed from the ocean surface. $\delta^{18}O_w$ in *P* seems to be reasonably well simulated. Unfortunately, we can ~~not~~ compare our simulated $\delta^{18}O_w$ in *E* to any observational data, but it could be that it is also slightly too enriched. Regarding the Arctic Ocean, except for the isotopic surface flux calculation as outlined above, i~~I~~nsufficient river discharge and neglecting the fractionation during sea ice formation could be further ~~possible~~ sources for the model-data deviations. As part of the Pan-Arctic River Transport of Nutrients, Organic Matter and Suspended Sediments (PARTNERS) project, Cooper et al. (2008) published flow-weighted annual mean discharge and $\delta^{18}O_w$ data (collected between 2003 and 2006) from the six largest Arctic rivers (Table 2). According to their estimates, $\delta^{18}O_w$ values of Eurasian rivers decrease from west-to-east, thus the Ob' river discharges the most enriched freshwater (-14.9 ‰) while the water of the Kolyma river is most depleted in heavy isotopes (-22.2 ‰). This west-to-east trend is also recognizable in our model (Fig. 139b), where the Ob' river contributes freshwater with a $\delta^{18}O_w$ value of around -15.6 ‰ and the Kolyma river of around -20.5 ‰. Even though it seems that the isotopic composition of the Ob' river is ~~overestimated~~too depleted, all the other three Russian rivers are not as depleted as seen in the PARTNERS data.

Measurements of the Yukon and Mackenzie rivers reveal intermediate isotopic signals (-20.2 ‰ and -19.1 ‰ respectively). In the MITgcm these signals are slightly more enriched with $\delta^{18}O_w$ values of around -17.1~~9.5~~ ‰ and -18.9 ‰ for the Yukon and Mackenzie rivers respectively. A consideration of ~~Comparing~~ the overall river discharge ~~in~~to the Arctic Ocean~~,~~ reveals a slight underestimation as the flow-weighted average for all six rivers is -18.8 ‰, while in the model it is only -18.0~~7.9~~ ‰. Not only does the isotopic signal of the river discharge matter, but also the discharge amount. Estimating the annual discharge amount

in the MITgcm is difficult, because determining the grid cells that belong to the respective river is based on visually assigning ~~dividing~~ them according to the ~~current~~ location of the river mouth. This may lead to deviations compared to observational data. While simulated annual discharge for the Yenisey, Lena, Yukon and Mackenzie rivers is in good agreement with reported values by Cooper et al. (2008 – Table 2), the amounts discharged by the Ob' and Kolyma rivers differ substantially. However, deviations of the annual discharge for all six rivers are tolerable (~ 400 $km^3\ a^{-1}$). Cooper et al. (2008) further reported that the Arctic Ocean basin receives 10 % of the global river runoff (1.3 Sv – Trenberth et al., 2007). The MITgcm fits right into this magnitude with 9.3 % of the simulated global river runoff (1.17 Sv) received by the Arctic Ocean (> 60° N). Thus, the deviations that appeared for the Ob' and Kolyma rivers are most likely attributable to the grid cell assignment~~division~~ described above and should not matter significantly. Therefore, both~~rather~~ the isotopic signal of ~~insufficient~~ river runoff and~~than~~ the discharge amount are rather insignificant for ~~is probably the source for~~ the model-data mismatch in the Arctic Ocean. ~~-~~The general pattern of the simulated isotopic river discharge shows that river runoff is more enriched in low and mid-latitudes (Fig. 913a), which is in accordance with observations (IAEA, 2012). Thus, simulating the isotopic composition of river runoff by taking the isotopic composition of the local precipitation is a reasonable first approximation, but should be overcome by implementing a bucket model in the MITgcm, which calculates the river discharge and its isotopic content for individual catchment areas over land.

Further discrepancies between model and observations might be due to the formation and transport of sea ice. During the formation of sea ice, the heavier isotopes are entrapped in the solid ice structure, while depleted sea ice brine is expelled (O'Neil, 1968). However, this fractionation process is relatively small. Lehmann and Siegenthaler (1991) reported an equilibrium fractionation constant of $2.91 \cdot 10^{-3}$ between pure water and ice under equilibrium laboratory conditions, while Melling and Moore (1995) estimated a fractionation constant of $2.09 \cdot 10^{-3}$ for ~1 m thick ice in the Canadian Beaufort Sea. So even though sea ice is highly dynamic, ~~since it forms in one location and melts somewhere else,~~ excluding not only the fractionation during the formation of sea ice but also the transportation of isotopes within the sea ice might lead to minor local changes but should not be one of the main sources of error. Indeed, Brennan et al. (2013) investigated the impact of a fractionation factor for sea ice on $\delta^{18}O_w$ ~~with~~in the University of Victoria Earth System Climate Model (UVic ESCM). They conclude that local changes in $\delta^{18}O_w$ due to the contribution of sea ice are smaller than 0.14 ‰ and therefore rather negligible. Furthermore, the coarse resolution of our model may cause~~trigger~~ some of the model-data discrepancies, since it is not able to resolve all of the physical processes. For instance, water that is transported towards the Nordic Seas as parts of the Gulf Stream System is displaced by water from the Labrador Sea due to the coarse horizontal grid system. Also, vertically the thermocline might not be as pronounced and located as in the real ocean, since e.g. the upper 500 m in the MITgcm are only represented by four layers. Observational data corresponding to depths within that transition layer might reflect a different signal than resolved by the ocean model.

Since $\delta^{18}O_w$ is a passive tracer, shifts at the ocean surface might propagate in the ocean interior. Errors in the general model performance might further add to the deviations in the deeper ocean. However, the water masses in the MITgcm in terms of structure, extent and magnitude are faithfully simulated (cf. 4.1) and thus can be ruled out as a significant error source.

Additionally, our isotopic forcing was not obtained from the same source as the atmospheric forcing for the freshwater, heat and momentum flux, whereby a maximum consistency cannot be ensured and an additional uncertainty to our sources of error is added.

Despite these sources of error, the simulated pattern of $\delta^{18}O_w$ both at the sea surface as well as in the deep ocean agrees fairly well with other recent studies such as the study by Xu et al. (2012) with an OGCM as well as the studies by Roche and Caley (2013) and Werner et al. (2016) with fully coupled models.

4.~~3~~2 Water mass structure

The seawater oxygen isotope ratio and salinity are controlled by the same processes such as evaporation, precipitation, river runoff and sea ice formation. In this way, they are locally linearly related, resulting in a slope that varies between 0.1 ‰ psu^{-1} in low latitudes and up to 1 ‰ psu^{-1} in high latitudes. However, water that is evaporated from the ocean surface does not carry any salt, but stable water isotopes. The agreement between the simulated slope and observational slope in the tropical regions is good, but significantly weaker in the mid-latitudes. This mismatch is mainly caused by the stable water isotopes since the overall comparison to observed SSS is quite good and comparable with other ocean models (cf. section 4.1).~~.~~ ~~With an RMSE of 0.45 psu our SSS results are comparable to Danabasoglu et al. (2012), who report an RMSE of 0.41 psu for the POP2 ocean component of the Community Climate System Model 4 (CCSM4) using a weak salinity restoring, and Griffies et al. (2011), who got an RMSE of 0.77 with the Geophysical Fluid Dynamics Laboratory Climate Model version 3.~~

Subtropical gyres are characterized by high salinity and $\delta^{18}O_w$ values. While the model shows reasonable salinities in these regions (Fig. 2a), its surface water is too depleted (Fig. ~~4~~3a). As discussed in section 4.2 theses discrepancies rather stem from an interaction of reduced *E* whereby not enough ^{16}O is removed from the ocean surface, $\delta^{18}O_w$ in *E* that is probably slightly too enriched and the dilutional effect of enhanced *P*.~~Either the precipitation is isotopically too depleted or water evaporating from the ocean surface is too enriched, whereby surface water is not enriched enough.~~ As opposed to this are the values of low salinity and $\delta^{18}O_w$ at the other end of the slope. They are mainly located around the upper boundary of the mid-latitudes (~ 60° N/S) near the coast (e.g. the Okhotsk Sea and Bering Sea) and within the western boundary currents (e.g. Gulf Stream). While the modeled salinity is slightly too salty, the $\delta^{18}O_w$ values are not as depleted as seen in observations, causing the deviations in the slope of the $\delta^{18}O_w$-salinity relationship. We infer, that the coarse grid resolution is the main driver for this mismatch.

~~Again, simulated salinity values are reasonable, but $\delta^{18}O_w$ values are not as depleted as seen in observations. Since these values are mainly located around the upper boundary of the mid-latitudes (~ 60 °N/S) near the coast, (e.g. the Okhotsk Sea and Bering Sea) and within the western boundary currents (e.g. Gulf Stream), we infer that the isotopic composition of river runoff and coarse grids resolution areis the main drivers for this mismatch.~~

Despite these discrepancies at the sea surface, the investigation of the water mass structure of the deeper parts of the ocean reveals that the model is suitable to determine the ~~large-scale~~large-scale distribution of water masses in terms of the $\delta^{18}O_w$ signature. Water mass formation regions are mainly located in the high-latitude Atlantic Ocean and produce large parts of the

deep and bottom waters of the ~~world~~ World ~~ocean~~Ocean. Hence, our investigation focuses on the main water masses (AAIW, AABW and NADW) within that basin. Emery and Meincke (1986) used published temperature and salinity data to determine the core properties of the main water masses of the W~~w~~orld O~~o~~cean. Applying these characteristics of the Atlantic Ocean to both the GISS data and modeled values (Fig. 1~~4~~0; Table 3~~2~~1), clearly shows the resemblance. All three water masses are found in the ocean model, but their temperature-salinity ranges differ slightly from those given by Emery and Meincke (1986) as discussed in section 4.1. ~~Both, NADW and AABW are slightly saltier in the model, while the later probably being colder too. AABW also seems to be colder.~~ Nevertheless, even though the absolute range of $\delta^{18}O_w$ values is narrower in the model than in the observations, the modeled mean values are remarkably close to the observations (cf. Table ~~2~~3~~1~~). Our results are quite encouraging, ~~particularly with regard to~~suggesting that the nonlinear free surface and real freshwater flux boundary conditions of the MITgcm ~~provides and are an~~ indeed leads to an improvement compared to other ocean models using salinity restoring (e.g. Paul et al., 1999; Xu et al., 2012).

Overall, even though some regions at the surface reveal localized biase~~d spots~~ regarding the $\delta^{18}O_w$ distribution, the water mass structure of the deeper parts of the ocean and their characteristic $\delta^{18}O_w$ values are successfully simulated. Hence, the ocean model is well suited to perform long-term simulations in a paleoclimatic context and investigating the respective $\delta^{18}O_w$ changes.

4.~~3~~ Planktonic foraminiferal $\delta^{18}O_c$

To address questions regarding the evolution and history of the ocean and climate, oxygen isotopic records derived from measurements of foraminiferal shells have been used extensively. Particularly, the last glacial maximum (LGM) and last deglaciation are time periods, for which the evidence comes from proxy data recorded as oxygen isotopes in $CaCO_3$. Hence, before using the model for paleostudies, an evaluation of modeled and measured $\delta^{18}O_c$ for the PI climate is necessary.

The $\delta^{18}O_c$ of planktonic foraminifera is not only determined by $\delta^{18}O_w$ and temperature of the ambient water in which the calcification takes place, but also altered by vital effects and modifications after death. Vital effects involve, for example, the photosynthetic activity of algal symbionts. Species like *G. ruber* (w) and *G. sacculifer* harbour symbionts (Kucera, 2007) that change the microenvironment around the shell by increasing the calcification rates through CO_2 uptake and thus shifting the pH towards more alkaline conditions corresponding to elevated carbonate ion concentrations ($[CO_3^{2-}]$). This mechanism will induce a kinetic fractionation that leads to relatively ^{18}O-depleted shells (Ravelo and Hillaire-Marcel, 2007). Furthermore, in the course of ontogenesis~~y~~ successive shell chambers reveal more enriched $\delta^{18}O_c$ values (Bemis et al., 1998), while significant changes also occur during reproduction. Bé (1980), Duplessy et al. (1981) and Mulitza et al. (2004) as well as others argue that some planktonic foraminifera add an additional layer of calcite during reproduction (gametogenic calcification). This additional calcite layer is secreted in deeper and cooler water masses, introducing an ^{18}O enrichment in the shell. Duplessy et al. (1981) ascertained a $\delta^{18}O$ mean enrichment of 0.78 ‰ and 0.92 ‰ in the shells of *G. ruber* and *G. sacculifer* from core-top sediments, respectively. Mulitza et al. (2004) also showed that foraminiferal shells from the sediment are increased in $\delta^{18}O$ by approximately 0.5-1 ‰. The average $\delta^{18}O$ composition recorded by a foraminiferal species at the sea floor ~~Shell composition i~~is further influenced not only by the vertical migration within the water column, whereby signals from different depths are

incorporated into the foraminiferal shell, but also by seasonal variations in shell production. Species that~~, which~~ prefer polar waters (e.g. *N. pachyderma* (s)) rather peak during summer, whereas species that~~, which~~ are distributed in warm provinces (e.g. *G. bulloides*) reflect a spring signal followed by a smaller autumn peak (Kucera, 2007). Additionally, the isotopic composition of foraminiferal shells can also be altered after deposition due to dissolution. This is especially the case, if the initial shell is dissolved rather than the crust formed during gametogenesis (gametogenic calcite is often more resistant to dissolution (Bé et al., 1975)), further shifting the $\delta^{18}O$ towards higher values.

All these mechanisms described above cannot be captured in our model, because it does not have an ecosystem module included, which could represent the life cycle of foraminifera and factors that determine the incorporation of oxygen isotopes in foraminiferal shells. Neglecting these processes might lead to additional model-data discrepancies. To avoid them,~~is~~ a comparison with plankton ~~-~~tow data is more reliable for testing the general capability of the model to simulate $\delta^{18}O_c$~~, for the first time,~~ since the depth and month of sampling is known (thus excluding any deviations due to seasonality or depth habitat) and the foraminifera are sampled alive (thus excluding any deviations due to gametogenic calcification or modifications after death).

For the surface distribution of $\delta^{18}O_c$, the largest discrepancies between model and data occurred in the Arctic Ocean. While the SST is too low, the $\delta^{18}O_w$ is not depleted enough in this region. These two effects could compensate each other, but the $\delta^{18}O_c$ reveals a slight overestimate, which results from the underestimated SST. To disentangle the background of any model-data mismatch it is best to investigate the model-data fit considering individual species (Fig. 15). Therefore, we use species~~-~~-specific paleotemperature equations published by Mulitza et al. (2003 – Table 4). First, we notice that the correlation is weaker when individual species are considered compared to investigating them grouped together. The ~~B~~best model-data fit is captured for *G. bulloides* (r^2 = 0.72, RMSE = 0.65 ‰, n = 35), while it is significantly weaker for *N. pachyderma* ((s); r^2 = 0.41, RMSE = 0.71 ‰, n = 61). While the largest deviations for *N. pachyderma* (s) occur in the upper surface column, data points that deviate from the 1:1 line for the other three species mainly correspond to depths larger~~water columns deeper~~ than 100 m (not shown here). This becomes clearer, when the model-data comparison is carried out for data that only falls in the upper level (< 50 m) of the ocean model, resulting in a significant improvement of the RMSE and r^2 for *G. ruber* ((w); r^2 = 0.86, RMSE = 0.41 ‰), *G. sacculifer* (r^2 = 0.80, RMSE = 0.37 ‰) and *G. bulloides* (r^2 = 0.83, RMSE = 0.56 ‰), while the RMSE worsens for *N. pachyderma* ((s); r^2 = 0.46, RMSE = 0.89 ‰). Even though the sampling depth of the plankton tow data is known and ~~we compared those by~~ was used for interpolation~~ng them~~ to the respective grid cell, ~~one can assume~~we suppose that the $\delta^{18}O_c$ signal recorded by the living foraminifera rather corresponds to a shallower water depth (at least for the first three species mentioned before). Schiebel and Hemleben (2005) illustrated the average depth inhabited by planktonic foraminifera (cf. Fig. 2 therein). While *G. ruber* (w), *G. sacculifer* and *G. bulloides* inhabit the upper surface column (~ 25 m, ~ 40 m and ~ 50 m, respectively), *N. pachyderma* (s) lives on average in deeper parts (~ 90 m) and thus might confirm the assumption above. Another source of error may be the coarse vertical resolution of the model.

Overall, modeled $\delta^{18}O_c$ values can be compared to data successfully with a better result when all species are grouped together compared to individual species. Taking into account the processes that potentially affect t~~Being aware of the potential~~

mechanisms the $\delta^{18}O_c$ of foraminiferal shells might undergo and considering the species-specific influence by habitat depth and seasonality, a comparison with $\delta^{18}O_c$ measured on shells collected from sediment cores appears to be feasible in a future study., is applicable. Apart from a few data points (red circle – Fig. 8a) most of the modeled $\delta^{18}O_c$ values fall below the 1:1 line and thus are biased towards lower values (Fig. 8a). The outliers are all located in high latitudes in the Arctic Ocean, which is, as mentioned before, a critical area in our model. We checked whether the mismatch is caused by temperature or $\delta^{18}O_w$. The temperature difference between modeled values and the WOA13 for the respective grid cells is rather small (differences not bigger than 0.15 °C) and can be ruled out as the main driving factor for our enriched $\delta^{18}O_c$ values. However, $\delta^{18}O_w$ is mainly increased by more than 1 ‰ and thus certainly leads to increased $\delta^{18}O_c$ values. The reason for the systematic offset of our modeled values is rather a matter of choice of the applied paleotemperature equation. The paleotemperature equation from Mulitza et al. (2004) is derived from plankton-tow specimens.

Our systematic offset of 0.74 ‰ falls into the range of these observed values and thus supports the notion that oxygen isotope values from core-top and sediment data are generally much higher than their plankton-tow counterparts. Hence, we assume that the core-top and Late Holocene data contain the signal formed by gametogenic calcification, while our $\delta^{18}O_c$ values calculated with the paleotemperature equation of Mulitza et al. (2004) only represent surface water conditions. Furthermore, one has to keep in mind that we compare modeled annual mean values to measurements of foraminiferal shells that do not represent an annual average but likely contain a seasonal bias, which is not considered (Žarić et al., 2005).

The observed offset vanishes, when applying the often used paleotemperature equation from Shackleton (1974) to our simulated values and comparing them to the dataset of Waelbroeck et al. (2005) (Fig. 8b). The RMSE slightly improves, while the r^2 and the slope almost remain unchanged (Table 2). However, this is not surprising, since the equation established by Shackleton (1974) is based on the shells of the benthic foraminifera *Uvigerina spp*, which, according to Zahn et al. (1986), are relatively enriched in ^{18}O. They assume that a low pH and decreased carbonate ion concentration, due to their habitat, might cause this latter enrichment. Based on these outcomes, we suggest, when modeling $\delta^{18}O_c$ of planktonic foraminifera and their respective surface water conditions, it is more appropriated to use paleotemperature equations derived from plankton-tow data (e.g. Mulitza et al., 2004) or more recent culture experiments (e.g. Spero et al., 2003), particularly since processes that affect the $\delta^{18}O_c$ of core-top sediments (e.g. gametogenic calcification) are not simulated and the commonly used paleotemperature equations like Shackleton (1974) or Kim and O'Neil (1997) tend to overestimate SST.

We further checked the agreement between modeled $\delta^{18}O_c$ and a data set derived from plankton tows (Duplessy et al., 1981, Kahn and Williams (1981), Ganssen 1983, Bauch et al., 1997 and Mulitza et al., 2003). Indeed, the MITgcm nicely reflects the $\delta^{18}O_c$ of living specimens (Fig. 8c) with a RMSE of 0.49 ‰ (Table 2). This further supports our assumption that $\delta^{18}O_c$ values from core-top sediments are a mixture of shells calcified at different water depths rather than just a pure surface water signal.

We conclude that the modeled $\delta^{18}O_c$ values can be compared to data successfully, although data from core-top data are generally much higher. Nevertheless, the latitudinal gradients of surface waters are well preserved and thus simulating

~~temperature and $\delta^{18}O_w$ simultaneously in an ocean model provides a unique opportunity for questions regarding the climate changes.~~

5 Conclusions

Stable water isotopes have been successfully implemented in the MITgcm, using real freshwater and isotopic flux boundary conditions in conjunction with the non-linear free surface. The model captures well the broad pattern and magnitude of $\delta^{18}O$ in annual mean seawater, reflecting accurately regions of net evaporation. The most enriched surface water occurs in the subtropical gyre of the Atlantic Ocean, while the surface water in the Arctic Ocean is isotopically most depleted. However, the latter ocean basin is the one with largest model-data discrepancies. They mostly result from the absence of highly depleted precipitation and snow fall in areas covered by sea ice. ~~insufficient river runoff, which is simulated by using the isotopic composition of the local precipitation at the river mouth, but are also attributable to~~ a large extent to ~~the coarse resolution of the model.~~ The simulated $\delta^{18}O_w$-salinity relationship is in good agreement with observations in tropical regions but less so in mid-latitudes, due to the misrepresentation of $\delta^{18}O_w$ caused by the coarse grid resolution of the model as well as an interaction of *P*, *E* and $\delta^{18}O_w$ in *E*. But even though the $\delta^{18}O_w$ distribution at the sea surface reveals some deviations, the water mass structure of the deeper parts of the ocean and their characteristic $\delta^{18}O_w$ values are ~~remarkably~~ well captured in our model and show that $\delta^{18}O_w$ indeed can be used to characterize different water masses. Further, we tested simulated $\delta^{18}O_c$ against measurements of planktonic foraminiferal shells from plankton tow data. Again, the latitudinal gradients and large-scale patterns are faithfully reproduced. The ~~M~~model-data fit is better when all species are grouped together, compared to individual species and the largest discrepancies are most likely attributable to different depth habitats. ~~. However, we observed a systematic offset towards lower values in our modeled $\delta^{18}O_c$. Gametogenic calcification probably causes this offset, since it is recorded in core-top and Late Holocene data but does not apply to living foraminiferal shells and their respective sea surface conditions. Hence, we suggest it is more appropriated to use paleotemperature equations derived from plankton-tow data or more recent culture experiments to investigate the $\delta^{18}O_c$ of planktonic foraminifera. Furthermore, for~~For a better understanding ~~about~~of the factors that determine the recording of ~~the incorporation of~~ oxygen isotopes in foraminiferal shells~~, as well as their life cycle,~~ might be provided by ecosystem models including foraminifera ~~like the one from~~ (Fraile et al. (2008); ~~or~~ Lombard et al. (2009); Kretschmer et al. (2016)). ~~are needed.~~

The MITgcm and its newly developed stable water isotope package offer a great opportunity to perform long-term simulations in a paleoclimatic context and assimilating water isotopes with the adjoint method. Thus, investigations of not only the respective changes in $\delta^{18}O_w$ but also in foraminiferal $\delta^{18}O_c$ during the LGM or last deglaciation can be performed.

6 Code availability

The water isotope package incorporated in the MITgcm can be obtained by contacting the first author: R. Völpel (rvoelpel@marum.de). Additionally, a release of the package through the MITgcm repository will be prepared.

Appendix A

The MITgcm provides a scheme that balances the freshwater flux (net fluxes are set to zero) at each time step, preventing uncontrolled drifts in salinity and sea surface height caused by an imbalance in precipitation, evaporation and runoff. However, this scheme adversely affects the seasonality of the net surface freshwater flux.

Following Large et al. (1997), a precipitation correction factor $f_P(y)$ (a tracer specific precipitation correction factor $f_P^i(y)$) is implemented in the MITgcm and computed each year y, whereby the global freshwater flux (the global isotopic flux) is annually balanced.

The correction factor is applied to the precipitation field (tracer specific precipitation field), such that the precipitation throughout a model year y is given by:

$$P = f_P(y) \cdot P(y) \quad \text{A(1)}$$

$$P^i = f_P^i(y) \cdot P^i(y)$$

A(2)

The size of f_P ($f_P^i(y)$) depends on the change in volume of global ocean freshwater throughout a year ($\Delta V^F{}_y$) (change in the amount of the global isotopic tracer in the ocean throughout a year - $\Delta n^i{}_y$) and the volume of precipitation (falling on the ice-free ocean)(amount of tracer specific precipitation) and river runoff (amount of tracer specific river runoff) as an annual integral (V^P (n^{P^i}) and V^R (n^{R^i}), respectively). These values are used to compute the correction factor for the following year:

$$f_P(y+1) = f_P(y)\left(1 - \frac{\Delta V_y^F}{(V^P + V^R)}\right) \quad \text{A(3)}$$

$$f_P^i(y+1) = f_P^i(y)\left(1 - \frac{\Delta n_y^i}{(n^{P^i} + n^{P^i})}\right) \quad \text{A(4)}$$

If the change in volume of global ocean freshwater is positive (negative), the global salinity will decrease (increase) and the correction factor is decreased (increased) for the next year ($y+1$). For the tracer specific correction factor, it applies that a positive (negative) change in the amount of the global isotopic tracer leads to an increase (decrease) in global tracer concentration and thus a decreased (increased) tracer specific correction factor for the next year ($y+1$). Throughout the model integration changes are getting smaller resulting in a precipitation correction factor (tracer specific precipitation correction factor) that remains approximately constant at $f_P(y)$ = 1. 0014 after ~ 1500 model years ($f_P^{H_2^{16}O}(y) = 1.0241$ after ~ 600 model years and $f_P^{H_2^{18}O}(y) = 1.0253$ after ~ 1200 model years – (Fig. A1).

Formatiert: Schriftart: (Standard) +Textkörper (Times New Roman)
Formatiert: Schriftart: (Standard) +Textkörper (Times New Roman)
Formatiert: Schriftart: (Standard) +Textkörper (Times New Roman)
Formatiert: Schriftart: (Standard) +Textkörper (Times New Roman)
Formatiert: Schriftart: (Standard) +Textkörper (Times New Roman)
Formatiert: Schriftart: (Standard) +Textkörper (Times New Roman)
Formatiert: Schriftart: (Standard) +Textkörper (Times New Roman), 10 Pt.
Formatiert: Schriftart: (Standard) +Textkörper (Times New Roman), 10 Pt.
Formatiert: Schriftart: (Standard) +Textkörper (Times New Roman)
Formatiert: Schriftart: 10 Pt.
Formatiert: Schriftart: 10 Pt.
Formatiert: Schriftart: 10 Pt.
Formatiert: Schriftart: 10 Pt.
Formatiert: Schriftart: 10 Pt.
Formatiert: Schriftart: 10 Pt.
Formatiert: Schriftart: 10 Pt.
Formatiert: Schriftart: 10 Pt.
Formatiert: Schriftart: 10 Pt.
Formatiert: Schriftart: 10 Pt.
Formatiert: Schriftart: 10 Pt.
Formatiert: Schriftart: 10 Pt.
Formatiert: Schriftart: 10 Pt.
Formatiert: Schriftart: 10 Pt.
Formatiert: Schriftart: (Standard) +Textkörper (Times New Roman), 10 Pt.
Formatiert: Schriftart: (Standard) +Textkörper (Times New Roman)
Formatiert: Schriftart: (Standard) +Textkörper (Times New Roman)
Formatiert: Schriftart: (Standard) +Textkörper (Times New Roman)

Acknowledgments.

We would like to thank T. Tharammal for providing the isotopic data of NCAR IsoCAM and T. Kurahashi-Nakamura for providing the atmospheric forcing fields obtained with the adjoint model. Further, we would like to thank Martin Losch for his advice throughout the model development. Comments and suggestions by the three anonymous reviewers and the Editor highly improved the quality and clarity of the manuscript. This project was funded through the DFG Research Center/Center of Excellence MARUM – "The Ocean in the Earth System".

References

Adcroft, A., Hill, C., and Marshall, J.: Representation of topography by shaved cells in a height coordinate ocean model, Mon.Weather Rev., 125, 2293-2315, 1997.

Adcroft, A. and Campin, J.-M.: Rescaled height coordinates for accurate representation of free-surface flows in ocean circulation models, Ocean Model., 7, 269 - 284, doi:10.1016/j.ocemod.2003.09.003, 2004.

Adcroft, A., Campin, J.-M., Hill, C., and Marshall, J.: Implementation of an Atmosphere Ocean General Circulation Model on the Expanded Spherical Cube, Mon. Weather Rev., 132, 2845-2863, doi:10.1175/MWR2823.1, 2004a.

Adcroft, A., Hill, C., Campin, J., Marshall, J., and Heimbach, P.: Overview of the formulation and numerics of the MIT GCM, in: Proceedings of the ECMWF Seminar Series on Numerical Methods: Recent Developments in Numerical Methods for Atmosphere and Ocean Modelling, ECMWF, 139-149, 2004b.

Baertschi, P.: Absolute ^{18}O content of standard mean ocean water, Earth Planet. Sc. Lett., 31, 341-344, doi:10.1016/0012-821X(76)90115-1, 1976.

Bauch, D., Carstens, J., and Wefer, G.: Oxygen isotope composition of living *Neogloboquadrina pachyderma* (sin.) in the Arctic Ocean, Earth Planet. Sc. Lett., 146, 47-58, doi:10.1016/S0012-821X(96)00211-7, 1997.

Bé, A. W. H.: Gametogenic calcification in a spinose planktonic foraminifer, *Globigerinoides sacculifer* (Brady), Mar. Micropaleontol., 5, 283-310, doi:10.1016/0377-8398(80)90014-6, 1980.

Bé, A. W. H., Morse, J. W., and Harrison, S. M.: Progressive dissolution and ultrastructural breakdown of planktonic foraminifera, in: Dissolution of Deep Sea Carbonates, edited by: Sliter, W. V., Bé, A. W. H., and Berger, W. H., Cushman Foundation for Foraminiferal Research, Special Publication, 13, 27-55, 1975.

Bemis, B. E., Spero, H. J., Bijma, J., and Lea, D. W.: Reevaluation of the oxygen isotopic composition of planktonic foraminifera: Experimental results and revised paleotemperature equations, Paleoceanography, 13, 150-160, doi: 10.1029/98PA00070, 1998.

Berry, D. I. and Kent, E. C.: A New Air-Sea Interaction Gridded Dataset from ICOADS with Uncertainty Estimates, B. Am. Meteorol. Soc., 90, 645-656, doi:10.1175/2008BAMS2639.1, 2009.

Brennan, C. E., Meissner, K. J., Eby, M., Hillaire-Marcel, C., and Weaver, A. J.: Impact of sea ice variability on the oxygen isotope content of seawater under glacial and interglacial conditions, Paleoceanography, 28, 388-400, doi:10.1002/palo20036, 2013.

Cooper, L.W., McClelland, J. W., Holmes, R. M., Raymond, P. A., Gibson, J. J., Guay, G. K., and Peterson, B. J.: Flow-weighted values of runoff tracers ($\delta^{18}O$, DOC, BA, alkalinity) from the six largest Arctic rivers, Geophys. Res. Lett., 35, L18606, doi:10.1029/2008GL035007, 2008.

Craig, H. and Gordon, L. I.: Deuterium and oxygen 18 variations in the ocean and the marine atmosphere, edited by: Tongiogi, El., Consiglio nazionale delle richerche, Laboratorio de geologia nucleare, Spoleto, Italy, 9-130, 1965.

Danabasoglu, G., Bates, S. C., Briegleb, B. P., Jayne, S. R., Jochum, M., Large, W. G., Peacock, S., and Yeager, S. G.: The CCSM4 Ocean Component, J. Climate, 25, 1361-1389, doi:10.1175/JCLI-D-11-00091.1, 2012.

Dansgaard, W.: Stable isotopes in precipitation, Tellus, 16, 436-468, 1964.

Dansgaard, W., Johnsen, S. J., Moller, J., and Langway, C. C. J.: One thousand centuries of climatic record from Camp Century on the Greenland ice sheet, Science, 166, 377-381, doi:10.1126/science.166.3903.377, 1969. ~~Fleitmann, D., Burns, S. J., Mudelsee, M., Neff, U., Kramers, J., Mangini, A., and Matter, A.: Holocene Forcing of the Indian Monsoon Recorded in a Stalagmite from Southern Oman, Science, 300, 1737-1739, doi:10.1126/science.1083130, 2003.~~

Delaygue, G., Jouzel, J., and Dtay, J. C.: Oxygen 18-salinity relationship simulated by an oceanic general circulation model, Earth Planet. Sc. Lett., 178, 113-123, doi:10.1016/S0012-821X(00)00073-X, 2000.

de Wit, J. C., VanderStraaten, C. M., and Mook, W. G.: Determination of the absolute hydrogen isotopic ratio of V–SMOW and SLAP, Geostandard. Newslett., 4, 33-36, doi:10.1111/j.1751-908X.1980.tb00270.x, 1980.

Duplessy, J. C., Blanc, P. L., and Bé, A. W. H.: Oxygen-18 enrichment of planktonic foraminifera due to gametogenic calcification below the euphotic zone, Science, 213, 1247-1250, doi:10.1126/science.213.4513.1247, 1981.

Emery, W. J. and Meincke, J.: Global water masses: summary and review, Oceanol Acta, 9, 383-391, 1986.

Emiliani, C.: Pleistocene temperatures, J. Geol., 63, 538-578, 1955.

Epstein, S., Sharp, R. P., and Gow, A. J.: Antarctic ice sheet: stable isotope analyses of Byrd station cores and interhemispheric climatic implications, Science, 16, 1570-1572, doi:10.1126/science.168.3939.1570, 1970.

Errico, R. M.: What Is an Adjoint Model?, B. Am. Meteorol. Soc., 78, 2577-2591, doi:10.1175/1520-0477(1997)078<2577:WIAAM>2.0.CO;2, 1997.

Fleitmann, D., Burns, S. J., Mudelsee, M., Neff, U., Kramers, J., Mangini, A., and Matter, A.: Holocene Forcing of the Indian Monsoon Recorded in a Stalagmite from Southern Oman, Science, 300, 1737-1739, doi:10.1126/science.1083130, 2003.

Fraile, I., Schulz, M., Mulitza, S., and Kucera, M.: Predicting the global distribution of planktonic foraminifera using a dynamic ecosystem model, Biogeoscienes, 5, 891-911, doi:10.5194/bg-5-891-2008, 2008.

Ganachaud, A.: Large-scale mass transport, water mass formation, and diffusivities estimated from World Ocean Circulation Experiment (WOCE) hydrographic data, J. Geophys. Res., 108, 3213, doi:10.1029/2002JC001565, 2003.

Ganssen, G.: Dokumentation von küstennahem Auftrieb anhand stabiler Isotope in rezenten Foraminiferen vor Nordwest-Afrika, "Meteor"-Forschungsergebnisse 37C, 1-46, 1983.

Gat, J. R. and Gonfiantini, R. (Eds): Stable isotope hydrology: Deuterium and Oxygen-18 in the water cycle, Int. At. Energy Agency, Vienna, 1981.

Gent, P. R. and McWilliams, J. C.: Isopycnal Mixing in Ocean Circulation Models, J. Phys. Oceanogr., 20, 150-160, doi:10.1175/1520-0485(1990)020<0150:IMIOCM>2.0.CO;2, 1990.

Griffies, S. M., Biastoch, A., Böning, C., Bryan, F., Danabasoglu, G., Chassignet, E. P., England, M. H., Gerdes, R., Haak, H., Hallberg, R. W., Hazeleger, W., Jungclaus, J., Large, W. G., Madec, G., Pirani, A., Samuels, B. L., Scheinert, M., Gupta, A. S., Severijns, C. A., Simmons, H. L., Treguier, A. M., Winton, M., Yeager, S., and Yin J.: Coordinated Ocean-ice Reference Experiments (COREs), Ocean Model., 26, 1-46, doi:10.1016/j.ocemod.2008.08.007, 2009.

Griffies, S. M., Winton, M., Donner, L. J., Horowitz, L. W., Downes, S. M., Farneti, R., Gnanadesikan, A., Hurlin, W. J., Lee, H.-C., Liang, Z., Palter, J. B., Samuels, B. L., Witternberg, A. T., Wyman, B. L., Yin, J., and Zadeh, N.: The GFDL CM3 Coupled Climate Model: Characteristics of the Ocean and Sea Ice Simulations, J. Climate, 24, 3520-3544, doi:10.1175/2011JCLI3964.1, 2011.

Hartmann, D. L.: Global Physical Climatology, 1st edition, Volume 56, Academic Press, San Diego, 411 pp., 1994.

Huang, R. X.: Real freshwater flux as a natural boundary condition for the salinity balance and thermohaline circulation forced by evaporation and precipitation, J. Phys. Oceanogr., 23, 2428-2446, 1993.

Huffman, G. J., Adler, R. F., Arkin, P., Chang, A., Ferraro, R., Gruber, A., Janowiak, J., McNab, A., Rudolf, B., and Schneider, U.: The Global Precipitation Climatology Project (GPCP) Combined Precipitation Dataset, B. Am. Meteorol. Soc., 78, 5-20, 1997.

Hundsdorfer, W. and Trompert, R. A.: Method of lines and direct discretization: a comparison for linear advection, Appl. Numer. Math., 13, 469-490, 1994.

Hut, G.: Stable Isotope Reference Samples for Geochemical and Hydrological Investigations. Consultant Group Meeting IAEA, Vienna, 16-18 September 1985, Report to the Director General, Internatinal Atomic Energy Agency, Vienna, Austria, 1987.

IAEA: Global Network of Isotopes in Rivers, available at: http://www-naweb.iaea.org/napc/ih/IHS_resources_gnir.html (last access: 31 August 2016), 2012.

Jackett, D. R. and McDougall, T. J.: Minimal adjustment of hydrographic profiles to achieve static stability, J. Atmos. Ocean. Tech., 12, 381-389, doi:10.1175/1520-0426(1995)012<0381:MAOHPT>2.0.CO;2, 1995.

Formatiert: Schriftart: (Standard) +Textkörper (Times New Roman)

Formatiert: Schriftart: (Standard) +Textkörper (Times New Roman)

Jacobs, S. S., Fairbanks, R. G., and Horibe, Y.: Origin and evolution of water masses near the Antarctic continental margin: Evidence from $H_2{}^{18}O/H_2{}^{16}O$ ratios in seawater, in: Oceanology of the Antarctic Continental Shelf edited by: Jacobs, S. S., vol. 43 of Antarctic Res. Ser., 59-85, AGU, Washington, D.C., doi:10.1029/AR043p0059, 1985.

Johnsen, S. J., Dansgaard, W., Clausen, H. B., and Langway, C. C.: Oxygen isotope profiles through the Antarctic and Greenland ice sheet, Nature, 235, 429-434, doi:10.1038/235429a0, 1972.

Johnsen, S. J., Dahl-Jensen, D., Gundestrup, N., Steffensen, J. P., Clausen, H. B., Miller, H., Masson-Delmotte, V., Sveinbjornsdottir, A. E., and White, J.: Oxygen isotope and palaeotemperature records from six Greenland ice-core stations: Camp Century, Dye-3, GRIP, GISP2, Renland and NorthGRIP, J. Quaternary Sci., 16, 299-307, doi:10.1002/jqs.622, 2001.

Joussaume, S., Sadourny, R., and Jouzel, J.: A general circulation model of water isotope cycles in the atmosphere, Nature, 311, 24-29, doi:10.1038/311024a0, 1984.

Jouzel, J., Russell, G. L., Suozzo, R. J., Koster, R. D., White, J. W. C., and Broecker, W. S.: Simulations of the HDO and $H_2{}^{18}O$ atmospheric cycles using the NASA GISS general circulation model: the seasonal cycle for present-day conditions, J. Geophys. Res., 92, 14739-14760, doi:10.1029/JD092iD12p14739, 1987.

Kahn, M. and Williams, D. F.: Oxygen and carbon isotopic composition of living planktonic foraminifera from the northeast Pacific Ocean, Palaeogeogr. Palaeocl., 33, 47-69, doi:10.1016/0031-0182(81)90032-8, 1981.

Keigwin, L., Bice, M., and Copley, N.: Seasonality and stable isotopes in planktonic foraminifera off Cape Cod, Massachusetts, Paleoceanography, 20, PA4011, doi:10.1029/2005PA001150, 2005.

Khatiwala, S. P., Fairbanks, R. G., and Houghton, R. W.: Freshwater sources to the coastal ocean off northeastern North America: Evidence from $H_2{}^{18}O/H_2{}^{16}O$, J. Geophys. Res., 104, 18,241-18,255, doi:10.1029/1999JC900155, 1999.

~~Kim, S. T. and O'Neil, J. R.: Equilibrium and nonequilibrium oxygen isotope effects in synthetic carbonates, Geochim. Cosmochim. Ac., 61, 3461-3475, 1997.~~Kohfeld, K. E. and Fairbanks, R. G.: *Neogloboquadrina pachyderma* (sinistral coiling) as paleoceanographic tracers in polar oceans: Evidence from Northeast Water Polynya plankton tows, sediment traps, and surface sediments, Paleoceanography, 11, 676-699, doi:10.1029/96PA02617 1996.

Kretschmer, K., Kucera, M., and Schulz, M.: Modeling the distribution and seasonality of *Neogloboquadrina pachyderma* in the North Atlantic Ocean during Heinrich Stadial 1, Paleoceanography, 31, 986-1010, doi:10.1002/2015PA002819, 2016.

Kucera, M.: Planktonic foraminifera as tracers of past oceanic environments, in: Developments in Marine Geology, Volume 1, Proxies in Late Cenozoic Paleoceanography, edited by: Hillaire-Marcel, C. and De Vernale, A., Elsevier, Amsterdam, 213-262, 2007.

Kurahashi-Nakamura, T., Paul, A., and Losch, M.: Dynamical reconstruction of the global ocean state during the Last Glacial Maximum, ~~submitted to~~ Paleoceanography, 32, doi:10.1002/2016PA003001, 2017~~6~~.

Large, W. G., Danabasoglu, G., Doney, S. C., and McWilliams, J. C.: Sensitivity to surface forcing and boundary layer mixing in a global ocean model: Annual-mean climatology, J. Phys. Oceanogr., 27, 2418-2447, doi:10.1175/1520-0485(1997)027<2418:STSFAB>2.0.CO;2, 1997.

Large, W. G. and Yeager, S. G.: Diurnal to decadal global forcing for ocean and sea-ice models: The data sets and flux climatologies, NCAR Technical Note, 4-15, doi:10.5065/D6KK98Q6, 2004.

Lehmann, M. and Siegenthaler, U.: Equilibrium oxygen- and hydrogen-isotope fractionation between ice and water, J. Glaciol., 37, 23-26, 1991.

Levitus, S. and Boyer, T.: World Ocean Atlas 1994, Vol. 4: Temperature, NOAA Atlas NESDIS 4, 1994.

Levitus, S., Burgett, R., and Boyer, T.: World Ocean Atlas 1994, Vol. 3: Salinity, NOAA Atlas NESDIS 3, 1994.

Locarnini, R. A., Mishonov, A. V., Antonov, J. I., Boyer, T. P., Garcia, H. E., Baranova, O. K., Zweng, M. M., and Johnson, D. R.: World Ocean Atlas 2009, Volume 1: Temperature, edited by: Levitus, S., NOAA Atlas NESDIS, 68, 184 pp., 2010.

Locarnini, R. A., Mishonov, A. V., Antonov, J. I., Boyer, T. P., Garcia, H. E., Baranova, O. K., Zweng, M. M., Paver, C. R., Reagan, J. R., Johnson, D. R., Hamilton, M., and Seidov, D.: World Ocean Atlas 2013, Volume 1: Temperature, edited by: Levitus, S., technical edited by: Mishonov, A., NOAA Atlas NESDIS, 73, 40 pp., 2013.

Lombard, F., Labeyrie, L., Michel, E., Speor, H., and Lea, D. W.: Modelling the temperature dependent growth rates of planktic foraminifera, Mar. Micropaleontol., 70, 1-7, 2009.

Losch, M., Menemenlis, D., Campin, J.-M., Heimbach, P., and Hill, C.: On the formulation of sea-ice models. Part 1: Effects of different solver implementations and parameterizations, Ocean Model., 33, 129-144, doi:10.1016/j.ocemod.2009.12.008, 2010.

Lumpkin, R., Speer, K., and Koltermann, K.: Transport across 48°N in the Atlantic Ocean, J. Phys. Oceanogr., 38, 733-752, doi:10.1175/2007JPO3636.1, 2008.

Majoube, M.: Fractionnement en oxygèn 18 et en deutérium entre l'eau et sa vapeur, Journal de Chimie et de Physique 68, 1423-1436, 1971.

Marshall, J., Adcroft, A., Hill, C., Perelman, L., and Heisey, C.: A finite-volume, incompressible Navier Stokes model for studies of the ocean on parallel computers, J. Geophys. Res., 102, 5753-5766, doi:10.1029/96JC02775, 1997.

Melling, H. and Moore, R. M.: Modification of halocline source waters during freezing on the Beaufort Sea shelf: evidence from oxygen isotopes and dissolved nutrients, Continent. Shelf Res., 15, 89-113, doi:10.1016/0278-4343(94)P1814-R, 1995.

Meredith, M. P., Heywood, K. J., Frew, R. D. and Dennis, P. F.: Formation and circulation of the water masses between the Southern Indian Ocean and Antarctica: Results from $\delta^{18}O$, J. Mar. Res., 57, 449-470, 1999.

Merlivat, L. and Jouzel, J.: Global climatic interpretation of the deuterium-oxygen 18 relationship for precipitation, J. Geophys. Res., 84, 5029-5033, doi:10.1029/JC084iC08p05029, 1979.

Moos, C.: Reconstruction of upwelling intensity and paleo-nutrient gradients in the northwest Arabian Sea derived from stable carbon and oxygen isotopes of planktic foraminifera, Ph.D. thesis, Faculty of Geosciences, University of Bremen, Bremen, Germany, 2000.

Mortyn, P. G. and Charles, C. D.: Planktonic foraminiferal depth habitat and $\delta^{18}O$ calibrations: Plankton tow results from the Atlantic sector of the Southern Ocean, Paleoceanography, 18, 15-1-15-14, doi:10.1029/2001PA000637, 2003.

Mulitza, S., Boltovskoy, D., Donner, D., Meggers, H., Paul, A., and Wefer, G.: Temperature: $\delta^{18}O$ relationships of planktic foraminifera collected from surface waters, Palaeogeogr. Palaeocl., 202, 143-152, doi:10.1016/S0031-0182(03)00633-3, 2003.

Mulitza, S., Donner, B., Fischer, G., Paul, A., Pätzold, J., Rühlemann, C., and Segl, M.: The South Atlantic oxygen-isotope record of planktic foraminifera, in: The South Atlantic in the Late Quaternary: Reconstruction of Mass Budget and Current Systems edited by Fischer, G. and Wefer, G., 121-142, Springer, New York, 2004.

O'Neil, J. R.: Hydrogen and oxygen isotopic fractionation between ice and water, J. Phys. Chem., 72, 3683-3684, doi:10.1021/j100856a060, 1986.

Paul, A., Mulitza, S., Pätzold, J., and Wolff, T.: Simulation of oxygen isotopes in a global ocean model, in: Use of proxies in paleoceanography: examples from the South Atlantic, edited by: Fisher, G. and Wefer, G., 655-686, Springer, Berlin, Heidelberg, Germany, 1999.

Peeters, F. J. C. and Brummer, G.-J. A.: The seasonal and vertical distribution of living planktonic foraminifera in the NW Arabian Sea, in: Tectonic and Climate Evolution of the Arabian Sea Region, Special Publication, 195, edited by: Clift, P., Kroon, D., Gaedicke, C., and Craig, J., Geological Society, London, 463-497, 2002.

Ravelo, C. and Hillaire-Marcel, C.: The use of oxygen and carbon isotopes of foraminifera in Paleoceanography, in: Developments in Marine Geology, Volume 1, Proxies in Late Cenozoic Paleoceanography, edited by: Hillaire-Marcel, C. and De Vernale, A., Elsevier, Amsterdam, 735-764, 2007.

Redi, M. H.: Oceanic Isopycnal Mixing by Coordinate Rotation, J. Phys. Oceanogr., 12, 1154-1158, doi:10.1175/1520-0485(1982)012<1154:OIMBCR>2.0.CO;2, 1982.

Rippert, N., Nürnberg, D., Raddatz, J., Maier, E., Hathorne, E., Bijma, J., and Tiedemann, R.: Constraining foraminiferal calcification depths in the western Pacific warm pool, Mar. Micropaleontol., 128, 14-27, doi:10.1016/j.marmicro.2016.08.004, 2016.

Roche, D. M. and Caley, T.: $\delta^{18}O$ water isotope in the *i*LOVECLIM model (version 1.0) – Part 2: Evaluation of the model results against observed $\delta^{18}O$ in water samples, Geosci. Model Dev., 6, 1493-1504, doi:10.5194/gmd-6-1493-2013, 2013.

Roche, D. M., Paillard, D., and Cortijo, E.: Constraints on the duration and freshwater release of Heinrich event 4 through isotopes modelling, Nature, 432, 379-382, 2004.

Rohling, E. J. and Bigg, G. R.: Paleosalinity and $\delta^{18}O$: a critical assessment, J. Geophys. Res., 103, 1307-1318, doi:10.1029/97JC01047, 1998.

Schiebel, R. and Hemleben, C.: Modern planktic foraminifera, Palaeont. Z., 79, 135-148, 2005.

Schmidt, G. A.: Oxygen-18 variations in a global ocean model, Geophys. Res. Lett., 25, 1201-1204, doi:10.1029/98GL50866, 1998.

Schmidt, G. A., BiggnG. R., and Rohling E. J.: Global seawater oxygen-18 database, available at: http://data.giss.nasa.gov/o18data (last access: 08 July 2016), 1999.

~~Shackleton, N. J.: Attainment of isotopic equilibrium between ocean water and the benthonic foraminifera genus Uvigerina: isotopic changes in the ocean during the last glacial, Gif-sur-Yvette, Colloque international du CNRS, 219,~~

Formatiert: Schriftart: (Standard) +Textkörper (Times New Roman)

Formatiert: Schriftart: (Standard) +Textkörper (Times New Roman)

203-210, 197Spero, H. J., Mielke, K. M., Kalve, E. M., Lea, D. W., and Pak, D. K.: Multispecies approach to reconstructing eastern equatorial Pacific thermocline hydrography during the past 360 kyr, Paleoceanography, 18, 1022, doi:10.1029/2002PA000814, 2003.Stangeew, E.: Distribution and isotopic composition of living planktonic foraminifera N. pachyderma (sinistral) and T. quinqueloba in the high latitude North Atlantic, Ph.D. thesis, Faculty of Mathematics and Natural Sciences, University of Kiel, Kiel, Germany, 2001.

Tharammal, T., Paul, A., Merkel, U., and Noone, D.: Influence of Last Glacial Maximum boundary conditions on the global water isotope distribution in an atmospheric general circulation model, Clim. Past, 9, 789-809, doi:10.5194/cp-9-789-2013, 2013.

Trenberth, K. E., Smith, L., Qian, T., Dai, A., and Fasullo, J.: Estimates of the Global Water Budget and Its Annual Cycle Using Observational and Model Data, J. Hydrometeorol., 8, 758-769, doi:10.1175/JHM600.1, 2007.

Volkmann, R. and Mensch, M.: Stable isotope composition ($\delta^{18}O$, $\delta^{13}C$) of living planktic foraminifers in the outer Laptev Sea and Fram Strait, Mar. Micropaleontol., 42, 163-188, doi:10.1016/S0377-8398(01)00018-4, 2001.

Wadley, M. R., Bigg, G. R., Rohling, E. J., and Payne, A. J.: On modelling present-day and last glacial maximum oceanic $\delta^{18}O$ distributions, Global Planet. Change, 32, 89-109, doi:10.1016/S0921-8181(01)00084-4, 2002.

Waelbroeck, C., Mulitza, S., Spero, H., Dokken, T., Kiefer, T., and Cortijo, E.: A global compilation of Late Holocene planktic foraminiferal $\delta^{18}O$: Relationship between surface water temperature and $\delta^{18}O$, Quaternary Sci. Rev. 24, 853-878, doi:10.1016/j.quascirev.2003.10.014, 2005.

Wang, Y. J., Cheng, H., Edwards, R. L., An, Z. S., Wu, J. Y., Shen, C. C., and Dorale, J. A.: A High-Resolution Absolute-Dated Late Pleistocene Monsoon Record from Hulu Cave, China, Science, 294, 2345-2348, doi:10.1126/science.1064618, 2001.

Werner, M., Haese, B., Xu, X., Zhang, X., Butzin, M., and Lohmann, G.: Glacial-interglacial changes in $H_2{}^{18}O$, HDO and deuterium excess – results frm the fully coupled ECHAM5/MPI-OM Earth system model, Geosci. Model Dev., 9, 647-670, doi:10.5194/gmd-9-647-2016, 2016.

Wilke, I., Meggers, H., and Bickert, T.: Depth habitats and seasonal distributions of recent planktic foraminifers in the Canary Islands region (29°N) based on oxygen isotopes, Deep Sea Research Part I: Oceanographic Research Papers, 56, 89-106, doi:10.1016/j.dsr.2008.08.001, 2009.

Xu, X., Werner, M., Butzin, M., and Lohmann, G.: Water isotope variations in the global ocean model MPI-OM, Geosci. Model Dev., 5, 809-818, doi:10.5194/gmd-5-809-2012, 2012.

Yi, Y., Gibson, J. J., Cooper, L. W., Helie, J.-F., Birks, S. J., Mccleland, J. W., Holmes, R. M., and Peterson, B. J.: Isotopic signals (^{18}O, ^{2}H, ^{3}H) of six major rivers draining the pam-Arctic watershed, Global Biogeochem. Cy., 26, GB1027, doi:10.1029/2011GB004159, 2012.

Zahn, R., Winn, K., and Sarnthein, M.: Benthic foraminiferal δ13C and accumulation rates of organic carbon: *Uvigerina peregrina* group and *Cibicidoides wuellerstorfi*, Paleoceanography, 1, 27-42, 1986.

~~Žarić, S., Donner, B., Fischer, G., Mulitza, S., and Wefer, G.: Sensitivity of planktic foraminifera to sea surface temperature and export production as derived from sediment trap data, Mar. Micropaleontol., 55, 75-105, doi:10.1016/j.marmicro.2005.01.002, 2005.~~

Zweng, M. M., Reagan, J. R., Antonov, J. I., Locarnini, R. A., Mishonov, A. V., Boyer, T. P., Garcia, H. E., Baranova, O. K., Johnson, D. R., Seidov, D., Biddle, M. M.: World Ocean Atlas 2013, Volume 2: Salinity, edited by: Levitus, S., technical edited by: Mishonov, A., NOAA Atlas NESDIS, 74, 39 pp., 2013.

Table 1: Main packages involved in the simulation of the stable water isotopes and their respective purposes.

Package	Purpose
Ptracers	initializes, advects and diffuses the passive tracers
Gchem	interface between the ptracers and wiso package → takes care of the additional sources and sinks for the passive tracers (e.g. surface forcing) by calling the respective wiso routines and adding the isotopic surface flux F^i to the tracer surface tendency $gPtr^i$
Wiso	calculates the isotopic evaporation E^i and surface flux F^i

Table 2: Annual mean $\delta^{18}O$ of river runoff and discharge for each of the six largest Arctic rivers presented by Cooper et al. (2008) and simulated by the MITgcm. Note that the river runoff in the MITgcm is distributed along the coasts (Fig. 9a and b) and thus the distinction which grid cell belongs to which river is just a rough approximation and can cause discrepancies.

River	$\delta^{18}O$ [‰] simulated by the MITgcm	$\delta^{18}O$ [‰] by Cooper et al. (2008)	Annual Discharge [$km^3\ a^{-1}$] simulated by the MITgcm	Annual Discharge [$km^3\ a^{-1}$] by Cooper et al. (2008)
Ob'	-15.6	-14.9	779	373
Yenisey	-17.7	-18.4	475	656
Lena	-19.8	-20.5	508	566
Kolyma	-20.5	-22.2	457	114
Yukon	-17.1	-20.2	172	214
Mackenzie	-18.9	-19.2	276	322

Formatiert: Schriftart: (Standard) +Textkörper (Times New Roman), 10 Pt., Nicht Fett
Formatiert: Schriftart: (Standard) +Textkörper (Times New Roman)
Formatiert: Schriftart: (Standard) +Textkörper (Times New Roman), 10 Pt., Nicht Fett
Formatierte Tabelle
Formatiert: Schriftart: (Standard) +Textkörper (Times New Roman), 10 Pt., Nicht Fett
Formatiert: Schriftart: (Standard) +Textkörper (Times New Roman)
Formatiert: Schriftart: (Standard) +Textkörper (Times New Roman), 10 Pt., Nicht Fett
Formatiert: Schriftart: (Standard) +Textkörper (Times New Roman), 10 Pt., Nicht Fett
Formatiert: Schriftart: (Standard) +Textkörper (Times New Roman), 10 Pt., Nicht Fett
Formatiert: Schriftart: (Standard) +Textkörper (Times New Roman)
Formatiert ...
Formatiert ...
Formatiert ...
Formatiert ...
Formatiert ...
Formatiert ...
Formatiert ...
Formatiert ...
Formatiert ...
Formatiert: Beschriftung
Formatiert ...
Formatiert ...
Formatiert: Beschriftung
Formatiert: Links
Formatierte Tabelle
Formatiert: Zentriert
Formatiert: Zentriert
Formatiert ...
Formatiert ...
Formatiert ...
Formatiert ...
Formatiert ...
Formatiert ...

All Six Rivers	-18.0	-18.8	2667	2245

Table 31: $\delta^{18}O_w$ characteristics of the main water masses (Antarctic Intermediate Water – AAIW, North Atlantic Deep Water – NADW and Antarctic Bottom Water – AABW) in the Atlantic Ocean for the observational (GISS) and simulated data (MIT). The $\delta^{18}O_w$ characteristics are determined by applying the temperature and salinity ranges of the respective water masses, reported by Emery and Meincke (1986), to the data within in the Atlantic Ocean (basin mask is based on the WOA09).

	AAIW	NADW	AABW
$\delta^{18}O_w^{GISS}$ range [‰]	-2.50 – 1.41	-0.49 – 0.88	-0.31 – 0.00
$\delta^{18}O_w^{GISS}$ mean value [‰]	-0.09	0.21	-0.14
$\delta^{18}O_w^{GISS}$ standard deviation [‰]	0.42	0.09	0.08
$\delta^{18}O_w^{MIT}$ range [‰]	-0.25 – 0.10	0.02 – 0.14	-0.16 – -0.03
$\delta^{18}O_w^{MIT}$ mean value [‰]	0.00	0.11	-0.11
$\delta^{18}O_w^{MIT}$ standard deviation [‰]	0.07	0.03	0.06

Table 42: Data-model comparison of $\delta^{18}O_c$ of planktonic foraminifera datas using species specific ~~different~~ palaeotenperature equations (Mulitza et al. (20034)~~, and Shackleton (1974)) and data sets (core-top and Late Holocene (LH) data (Waelbroeck et al., 2005) and living specimens (Duplessy et al., 1981, Kahn ans Williams (1981), Ganssen 1983, Bauch et al., 1997 and Mulitza et al., 2003)).~~

~~Data set~~Foraminiferal species	Palaeotemperature equation	RMSE [‰]	r^2	slope [‰ ‰$^{-1}$]
~~Core-top and LH data~~*G. ruber* (w)	~~$T\,[°C] = 14.32 - 4.28 \cdot (\delta^{18}O_c - \delta^{18}O_w) + 0.07 \cdot (\delta^{18}O_c - \delta^{18}O_w)^2$ (Mulitza et al., 2004)~~ $T = -4.44 \cdot (\delta^{18}O_c - \delta^{18}O_w) + 14.20$	0.891.01	0.419	0.771.03

~~Core-top and LH data~~*G. sacculifer*	~~$T\,[°C] = 16.90 - 4.38 \cdot (\delta^{18}O_c - \delta^{18}O_w) + 0.01 \cdot (\delta^{18}O_c - \delta^{18}O_w)^2$ (Shackleton, 1974)~~ $T = -4.35 \cdot (\delta^{18}O_c - \delta^{18}O_w) + 14.91$	0.81~~0.70~~	0.44~~0.9~~	0.97~~1.04~~
~~Living specimens~~*G. bulloides*	~~$T\,[°C] = 14.32 - 4.28 \cdot (\delta^{18}O_c - \delta^{18}O_w) + 0.07 \cdot (\delta^{18}O_c - \delta^{18}O_w)^2$ (Mulitza et al., 2004)~~ $T = -4.70 \cdot (\delta^{18}O_c - \delta^{18}O_w) + 14.62$	0.65~~0.49~~	0.71~~93~~	1.05~~1.06~~
G. pachyderma (s)	$T = -3.55 \cdot (\delta^{18}O_c - \delta^{18}O_w) + 12.69$	0.71	0.41	0.53

Formatiert: Schriftart: (Standard) +Textkörper (Times New Roman)

Formatiert: Schriftart: Kursiv

Formatiert: Schriftart: (Standard) +Textkörper (Times New Roman)

Formatiert: Schriftart: (Standard) +Textkörper (Times New Roman)

Formatiert: Schriftart: (Standard) +Textkörper (Times New Roman)

Formatiert: Schriftart: (Standard) +Textkörper (Times New Roman)

Formatiert: Schriftart: (Standard) +Textkörper (Times New Roman)

Formatiert: Schriftart: (Standard) +Textkörper (Times New Roman)

Formatiert: Schriftart: (Standard) +Textkörper (Times New Roman)

Formatierte Tabelle

Formatiert: Schriftart: (Standard) +Textkörper (Times New Roman)

Formatiert: Schriftart: (Standard) +Textkörper (Times New Roman)

Formatiert: Schriftart: (Standard) +Textkörper (Times New Roman)

Formatiert: Schriftart: (Standard) +Textkörper (Times New Roman)

Formatiert: Schriftart: (Standard) +Textkörper (Times New Roman), Kursiv

Formatiert: Schriftart: (Standard) +Textkörper (Times New Roman)

Formatiert: Schriftart: Nicht Kursiv

Formatiert: Schriftart: (Standard) +Textkörper (Times New Roman)

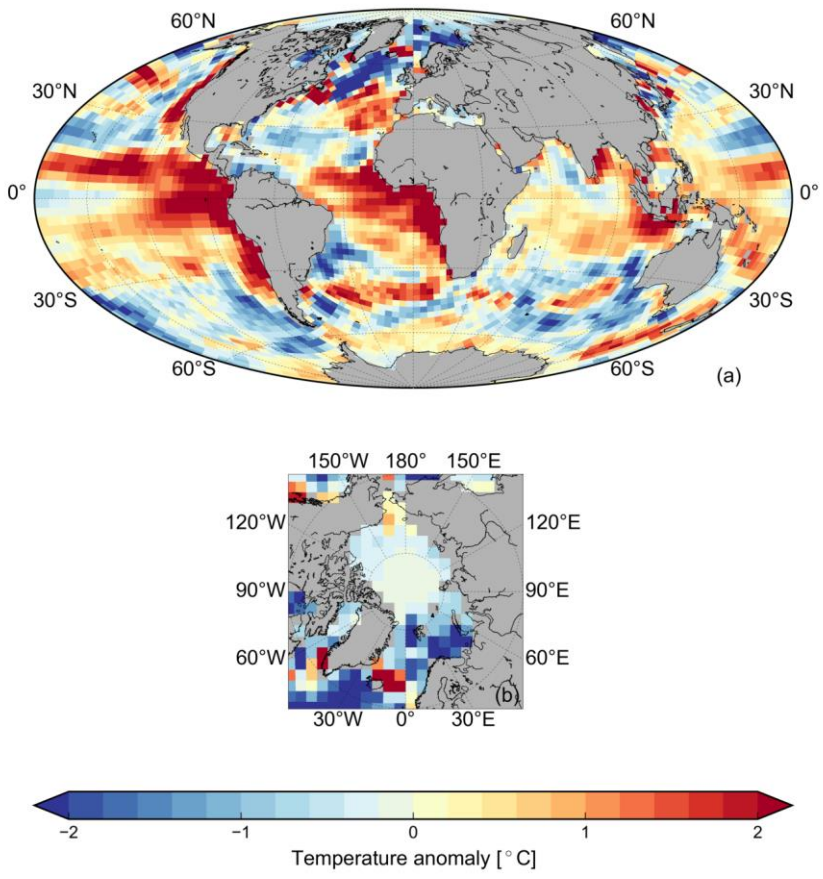

Figure 1: Annual mean sSea surface temperature anomaly (simulated in the MITgcm – WOA13, upper 50 m) for (a) the global ocean and (b) the Arctic Ocean. For the calculation of the anomaly the SST of the WOA13 was averaged over the upper 50 m and interpolated to the cubed sphere grid of the MITgcm.

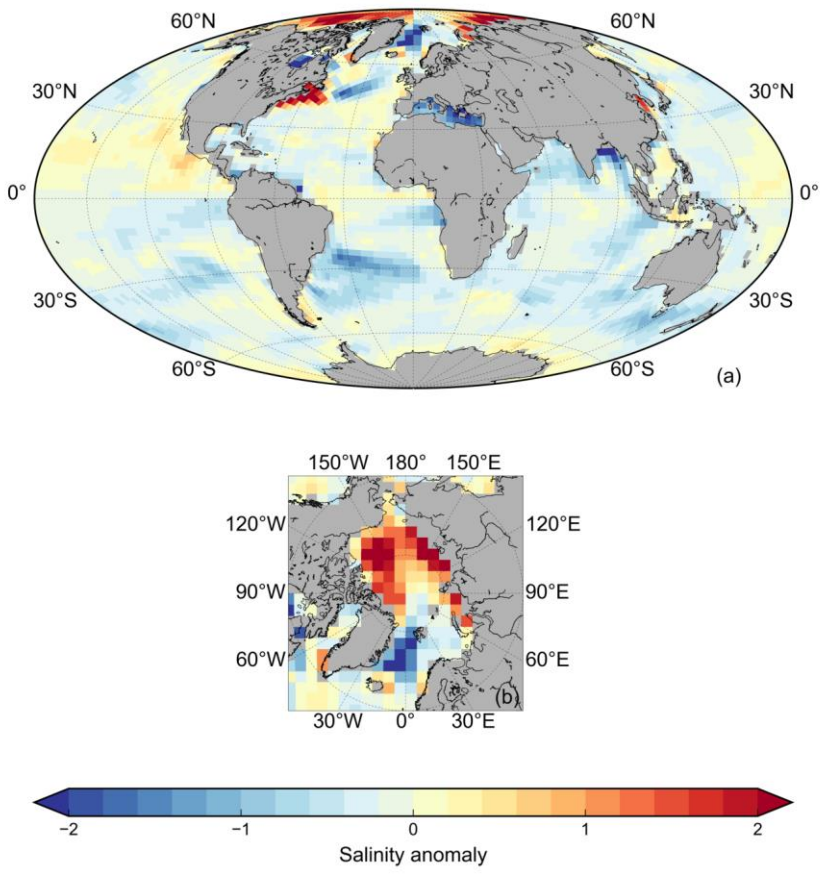
60°N
60°N
30°N
30°N
0°
0°
30°S
30°S
60°S
60°S
(a)
150°W
180°
150°E
120°W
120°E
90°W
90°E
60°W
60°E
30°W
0°
30°E
(b)
−2
−1
0
1
2
Salinity anomaly

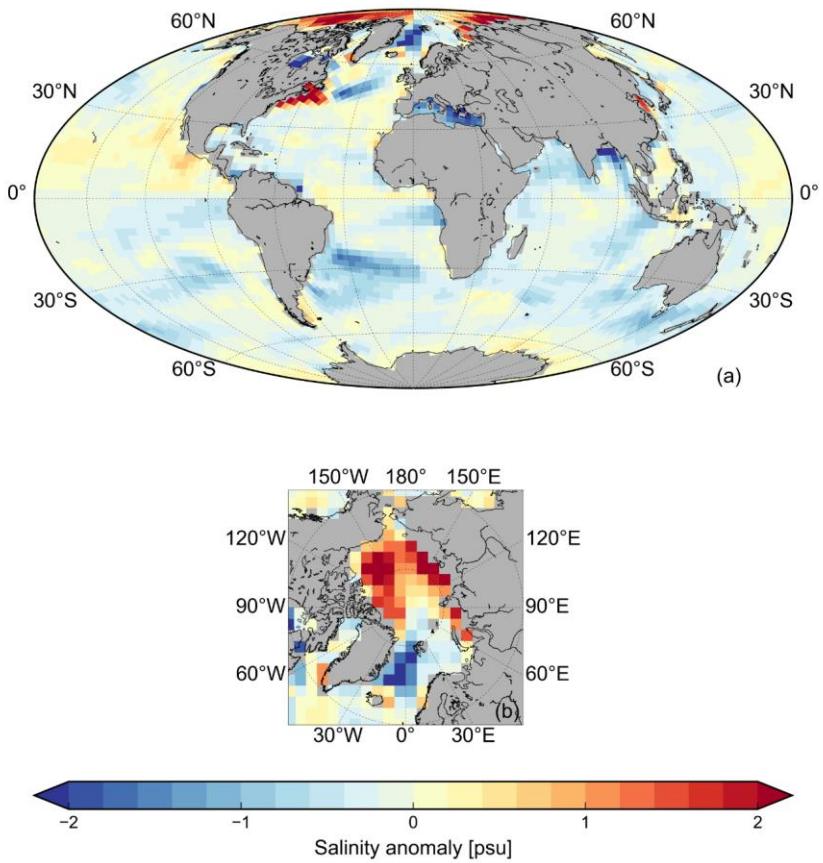

Figure 2: Annual mean ~~s~~Sea surface salinity anomaly (~~simulated in the~~ MITgcm – WOA13, upper 50 m) for (a) the global ocean and (b) the Arctic Ocean. For the calculation of the anomaly the SSS of the WOA13 was averaged over the upper 50 m and interpolated to the cubed sphere grid of the MITgcm.

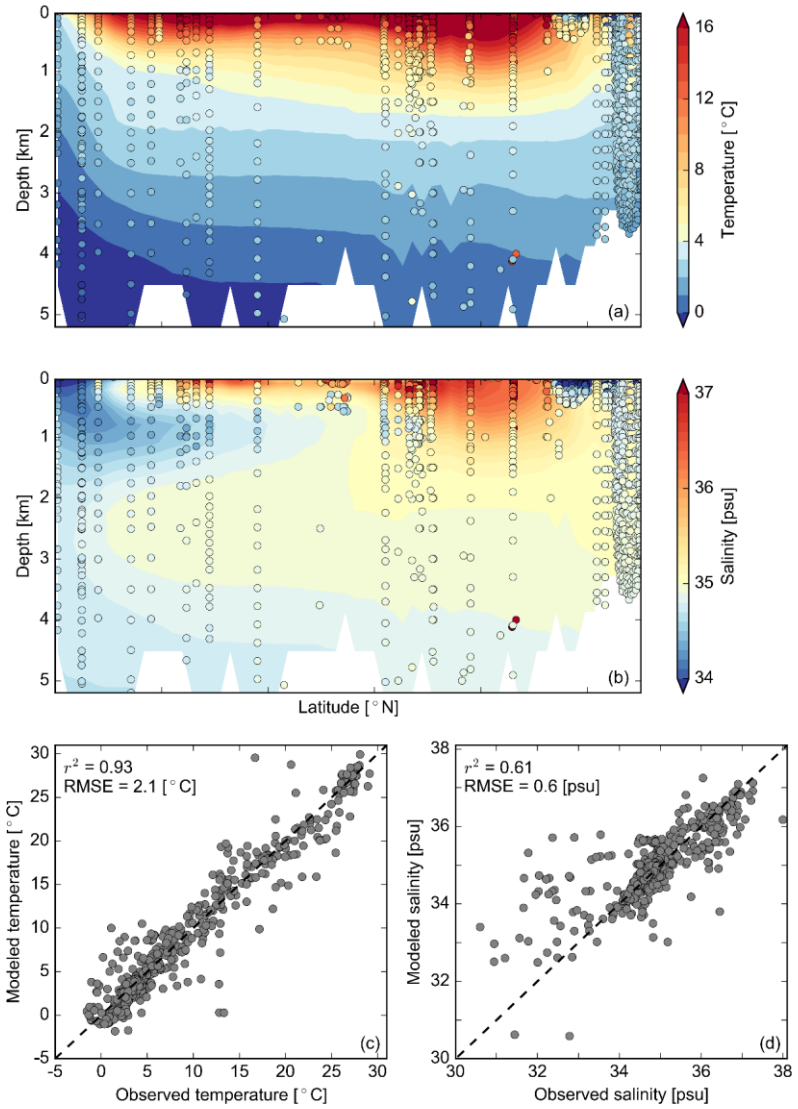
Depth [km]
0
1
2
3
4
5
(a)
16
12
8
4
0
Temperature [° C]
(b)
37
36
35
34
Salinity [psu]
Latitude [° N]
r^2 = 0.93
RMSE = 2.1 [° C]
Modeled temperature [° C]
Observed temperature [° C]
(c)
r^2 = 0.61
RMSE = 0.6 [psu]
Modeled salinity [psu]
Observed salinity [psu]
(d)

Figure 3: Zonally-averaged cross sections through the Atlantic Ocean for (a) the simulated annual mean temperature distribution and (b) the simulated annual mean salinity distribution in comparison to the observational GISS data (colored symbols – Schmidt et al., 1999; (a): n = 2234, (b): n = 2666). The zonal-averaged cross sections have been determined using the Atlantic basin mask provided by the WOA09 (Locarnini et al., 2010) and dividing it into equally spaced latitudinal bands along which a weighted zonal mean was calculated. Note that the GISS data does not represent a zonal mean, but rather values from specific locations taken at a certain time during the year. The relationship between the observed data and simulated long-term monthly mean temperature and salinity in the Atlantic Ocean is presented in (c) and (d) respectively. For the comparison, the specific month of GISS sampling has been considered. Dashed lines represent the 1:1 line.

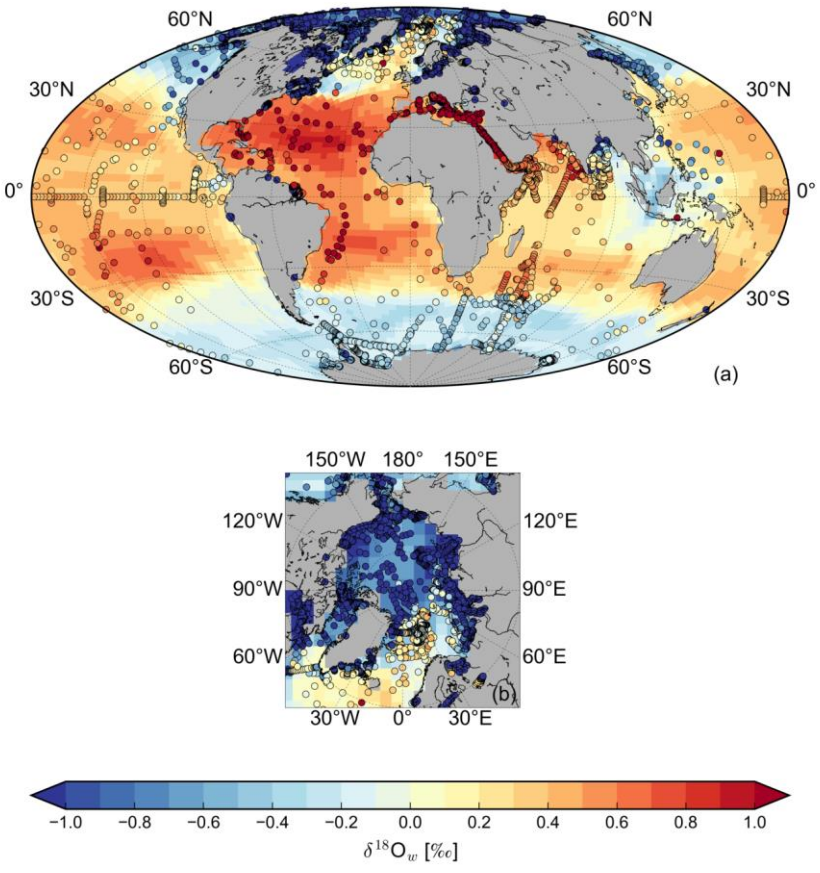
60°N
60°N
30°N
30°N
0°
0°
30°S
30°S
60°S
60°S
(a)
150°W
180°
150°E
120°W
120°E
90°W
90°E
60°W
60°E
30°W
0°
30°E
(b)
−1.0
−0.8
−0.6
−0.4
−0.2
0.0
0.2
0.4
0.6
0.8
1.0
$\delta^{18}O_w$ [‰]

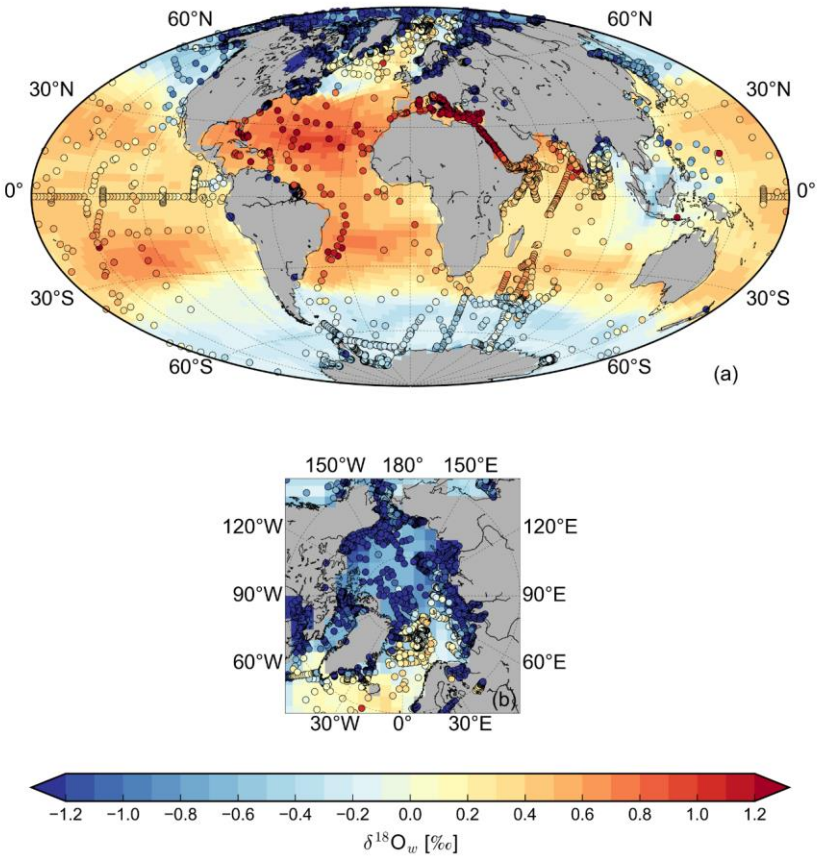

Figure 43: Global annual mean surface (upper 50 m) $\delta^{18}O_w$ distribution simulated by the MITgcm in comparison to the observational GISS data (colored symbols - (Schmidt et al., 1999) ~~– averaged over the upper 50 m~~) for (a) the global ocean and (b) the Arctic Ocean. The GISS data are averaged over the upper 50 m and do not represent an annual mean, but a certain time during the year.

Formatiert: Schriftart: (Standard) +Textkörper (Times New Roman)

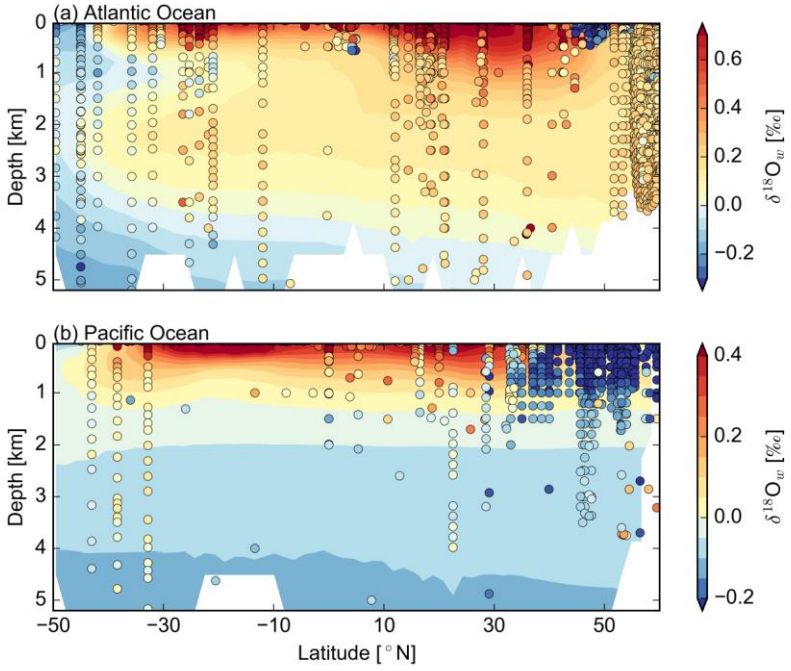

Figure 54: Zonally-averaged cross section for the simulated annual mean $\delta^{18}O_w$ distribution in (a) the Atlantic and (b) the Pacific Ocean in comparison to the observational GISS data (colored symbols – Schmidt et al., 1999; Atlantic Ocean: n = 2713, Pacific Ocean: n = 2929). The zonal-averaged cross sections have been determined using the respective basin masks provided by the WOA09 (Locarnini et al., 2010) and dividing it into equally spaced latitudinal bands along which a weighted zonal mean was calculated. Note that the GISS data does not represent a zonal mean, but rather values from specific locations taken at a certain time during the year.

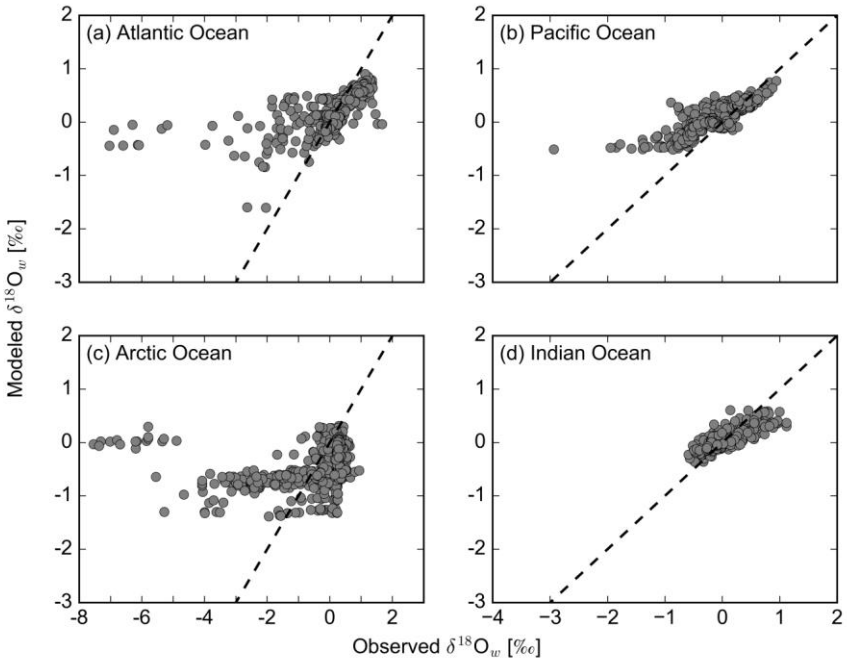
(a) Atlantic Ocean
(b) Pacific Ocean
(c) Arctic Ocean
(d) Indian Ocean
Modeled $\delta^{18}O_w$ [‰]
Observed $\delta^{18}O_w$ [‰]

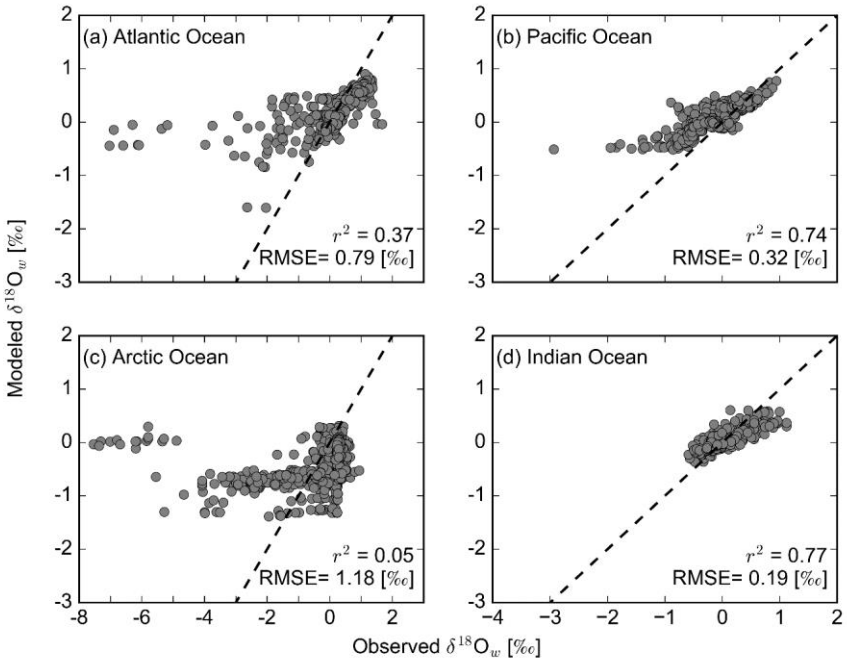

Figure 65: Relationship between observed $\delta^{18}O_w$ from the GISS database (Schmidt et al., 1999) and simulated long-term monthly mean $\delta^{18}O_w$ from the MITgcm for the different ocean basins: (a) Atlantic Ocean, (b) Pacific Ocean, (c) Arctic Ocean and (d) Indian Ocean. For the comparison, the specific month of GISS sampling has been considered. Dashed lines represent the 1:1 line.

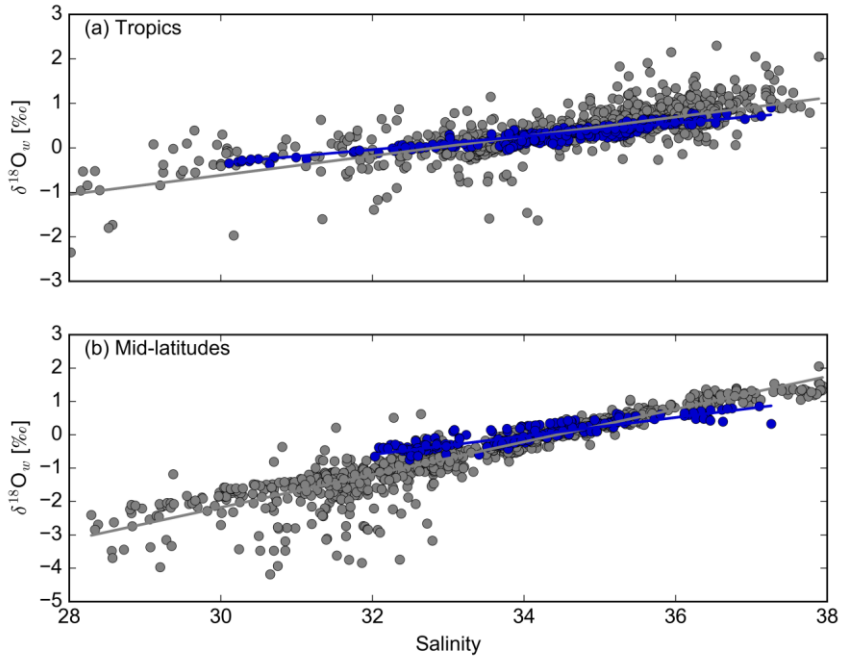
(a) Tropics
(b) Mid-latitudes
$\delta^{18}O_w$ [‰]
Salinity
3
2
1
0
−1
−2
−3
−4
−5
28
30
32
34
36
38

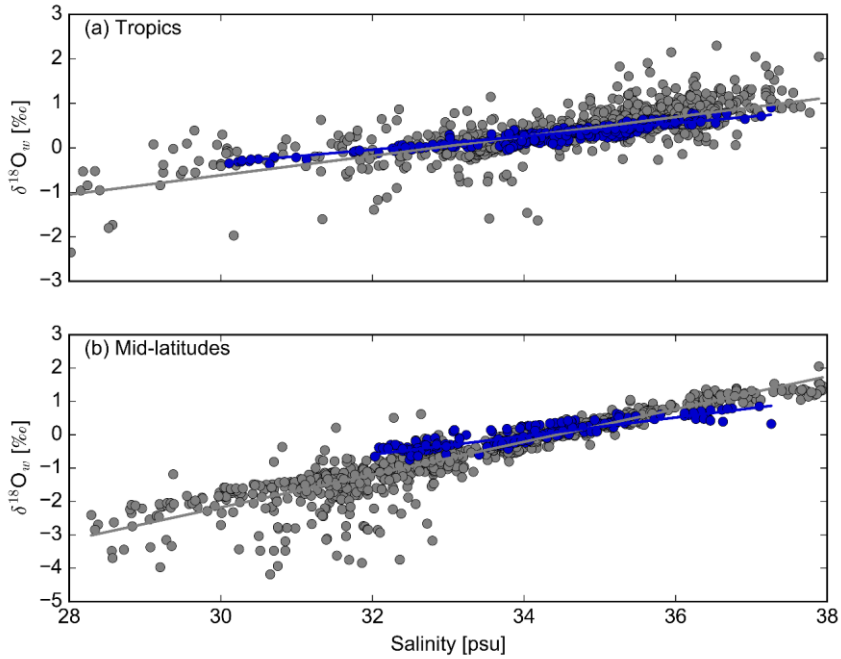

Figure 76: Salinity and $\delta^{18}O_w$ relation in surface waters (upper 50 m) for observational data (grey symbols – Schmidt et al., 1999) and simulated values (blue symbols) in (a) the tropics (25°S – 25°N) and (b) the mid-latitudes (25°S/N – 60°S/N). All GISS data in a depth range of 0-50 m with both salinity and $\delta^{18}O_w$ values available are presented (tropics: n = 1191, mid-latitudes: n = 1282), while the closest long-term monthly mean tracer grid value of salinity and $\delta^{18}O_w$ to the GISS datapoints of the respective month of sampling were chosen (tropics: n = 292, mid-latitudes: n = 245). The $\delta^{18}O_w$/salinity slopes are given in the text.

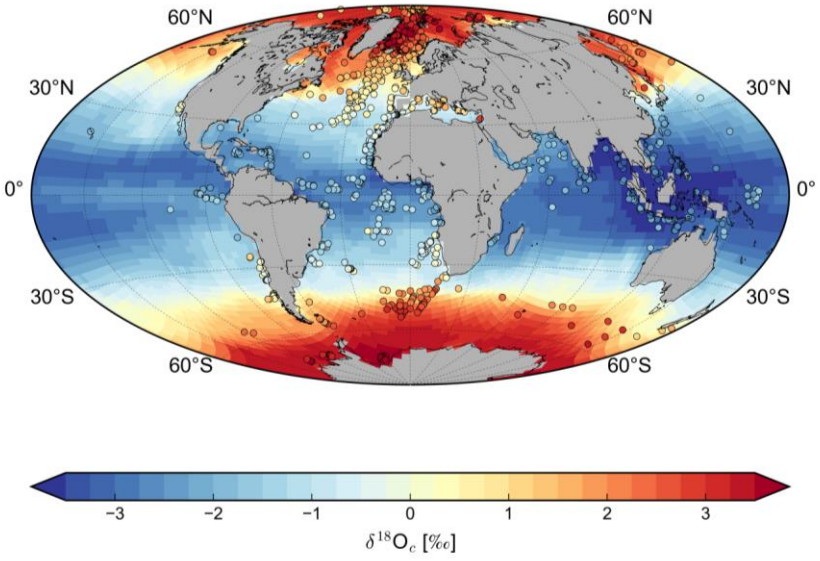
60°N
60°N
30°N
30°N
0°
0°
30°S
30°S
60°S
60°S
−3
−2
−1
0
1
2
3
$\delta^{18}O_c$ [‰]

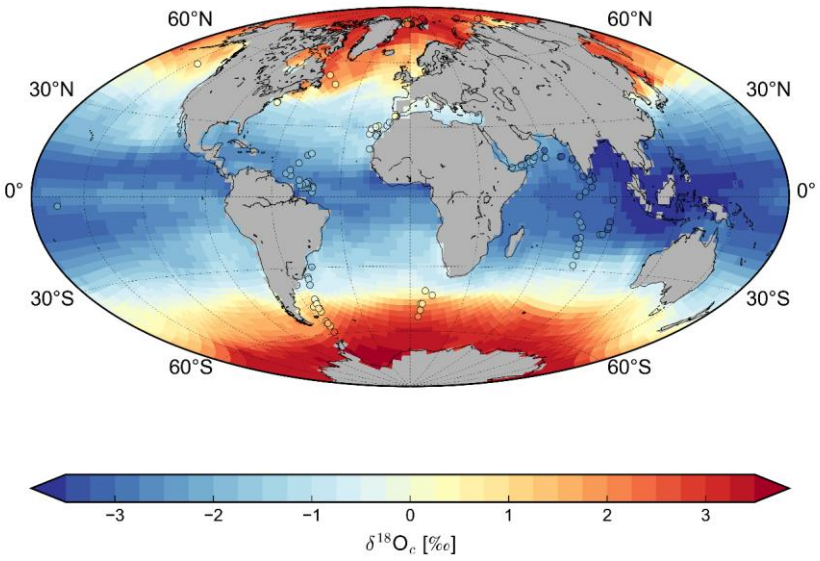

Figure 8~~7~~: Modeled annual mean sea surface $\delta^{18}O_c$ distribution (upper 50 m) compared to $\delta^{18}O_c$ values measured on planktonic foraminifera from plankton tows ~~core top and Late Holocene $\delta^{18}O_c$ from various planktonic foraminiferas~~ (colored symbols – for references see text). ~~– Waelbroeck et al., 2005~~). The plankton tow data are averaged over the upper 50 m and do not represent an annual mean, but a certain time during the year.

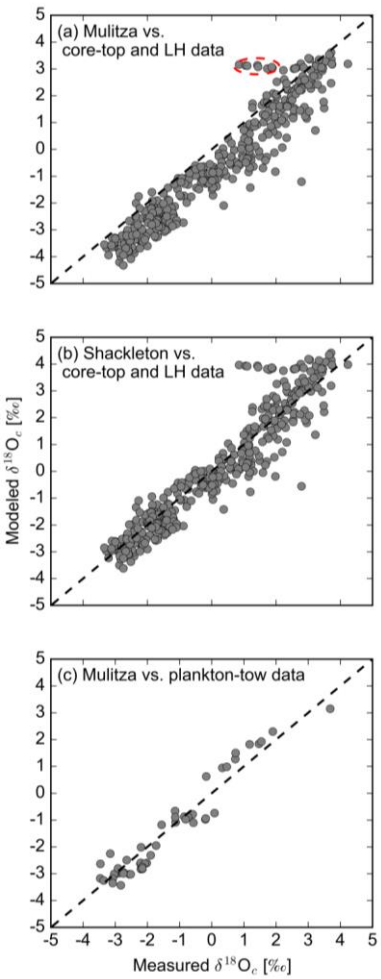
(a) Mulitza vs.
core-top and LH data
(b) Shackleton vs.
core-top and LH data
(c) Mulitza vs. plankton-tow data
Modeled $\delta^{18}O_c$ [‰]
Measured $\delta^{18}O_c$ [‰]

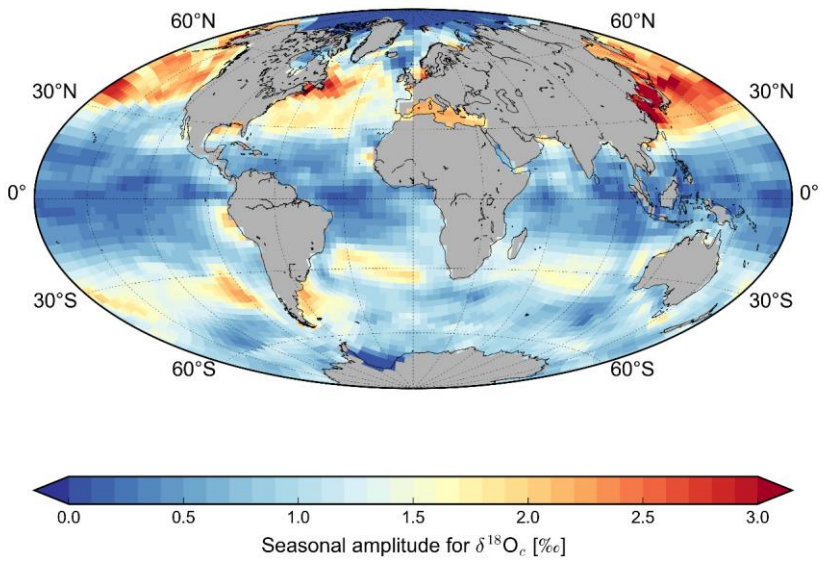

Figure 9: Simulated seasonal amplitude for $\delta^{18}O_c$ at the surface (upper 50 m). The seasonal amplitude is determined by calculating the absolute value between the two extreme months.

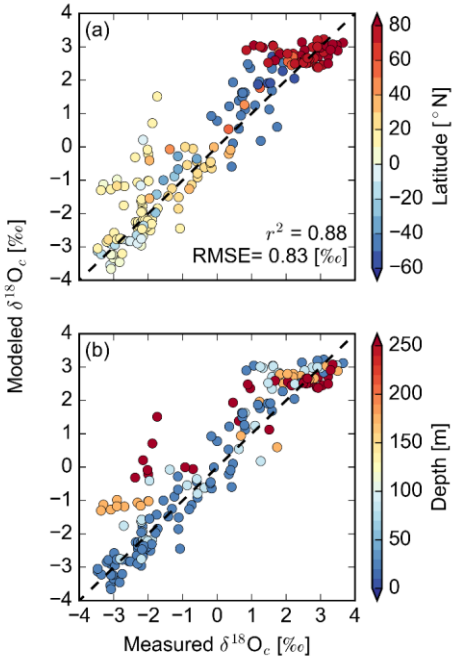

Figure 10: Relationship between measured $\delta^{18}O_c$ from various planktonic foraminiferas from plankton tows (for references see text) and simulated long-term monthly mean $\delta^{18}O_c$ from the MITgcm either depending on latitude (a) or depth (b). For the comparison, the specific month and depth of plankton tow sampling has been considered and plankton tow data was interpolated to the closest tracer grid cell of the model, using inverse distance weighting. Dashed lines represent the 1:1 line.

~~**Relationship between measured $\delta^{18}O_c$ from various planktonic foraminiferas (core-top and Late Holocene (LH) - Waelbroeck et al., 2005) and modeled annual mean $\delta^{18}O_c$ from the MITgcm using the paleotemperature equation from Mulitza et al., 2004 (a) and Shackleton, 1974 (b). The red circle in (a) marks data points that do not fit to the observed systematic offset. The relationship between measured $\delta^{18}O_c$ from plankton tows (Duplessy et al., 1981, Kahn and Williams (1981), Ganssen 1983, Bauch et al., 1997 and Mulitza et al., 2003) and modeled $\delta^{18}O_c$ from the MITgcm using the paleotemperature equation from Mulitza et al., 2004 is displayed in (c). Dashed lines represent the 1:1 line.**~~

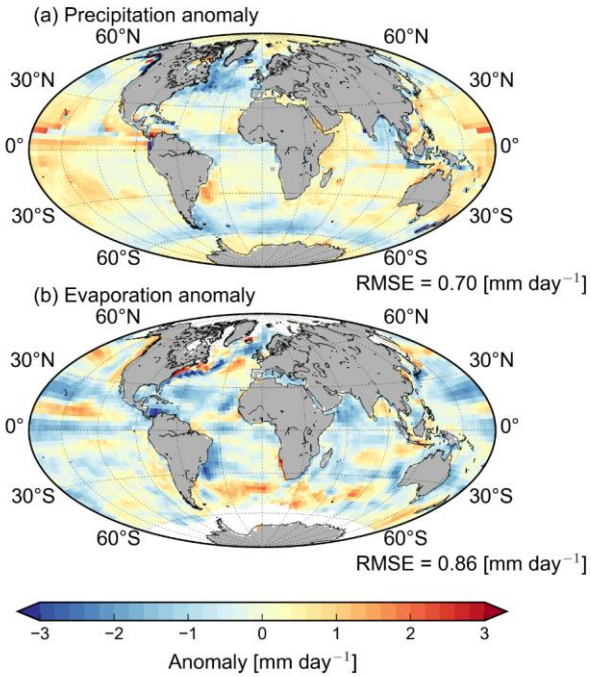

Figure 1~~1~~0: Annual mean precipitation (a) and evaporation (b) anomaly (MITgcm – observational data). The observed precipitation field is provided by GPCP (Huffmann et al., 1997), while the latent heat flux from the NOC Version 2.0 Surface Flux and Meteorological Dataset (Berry et al., 2009) is converted to evaporation and used for comparison.

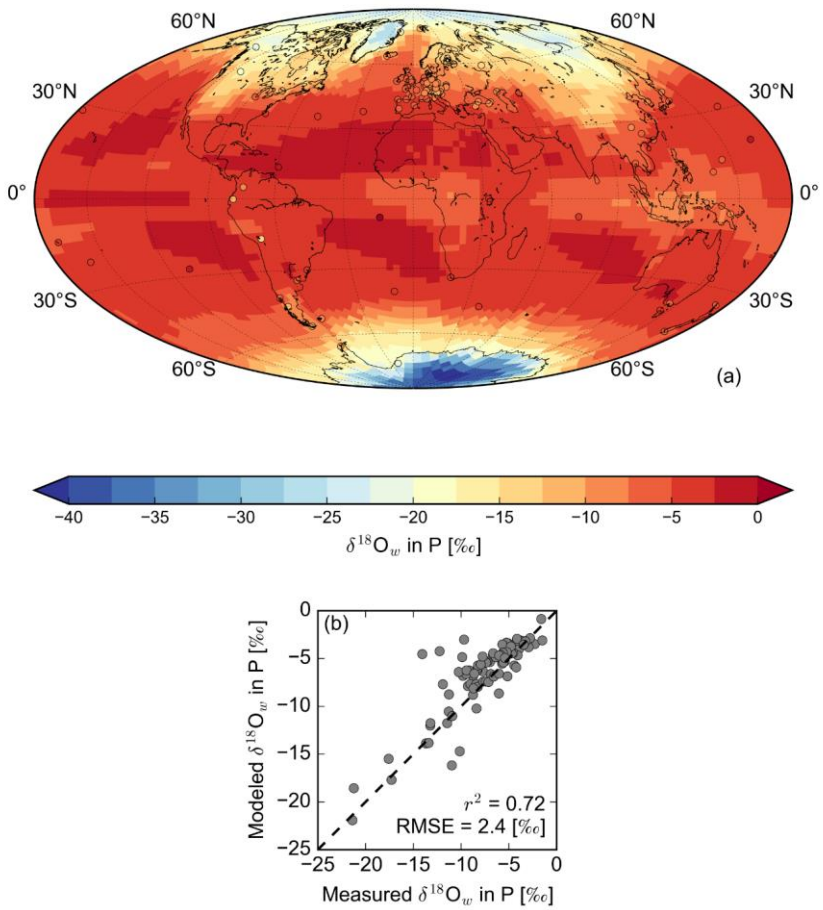

Figure 12: (a) Prescribed~~Modeled~~ annual mean isotopic composition in precipitation compared to GNIP data (colored symbols IAEA/WMO, 2010). (b) Model-data comparison of the annual mean values. GNIP data was interpolated to the closest tracer grid cell of the MITgcm, using inverse distance weighting. Dashed lines represent the 1:1 line.

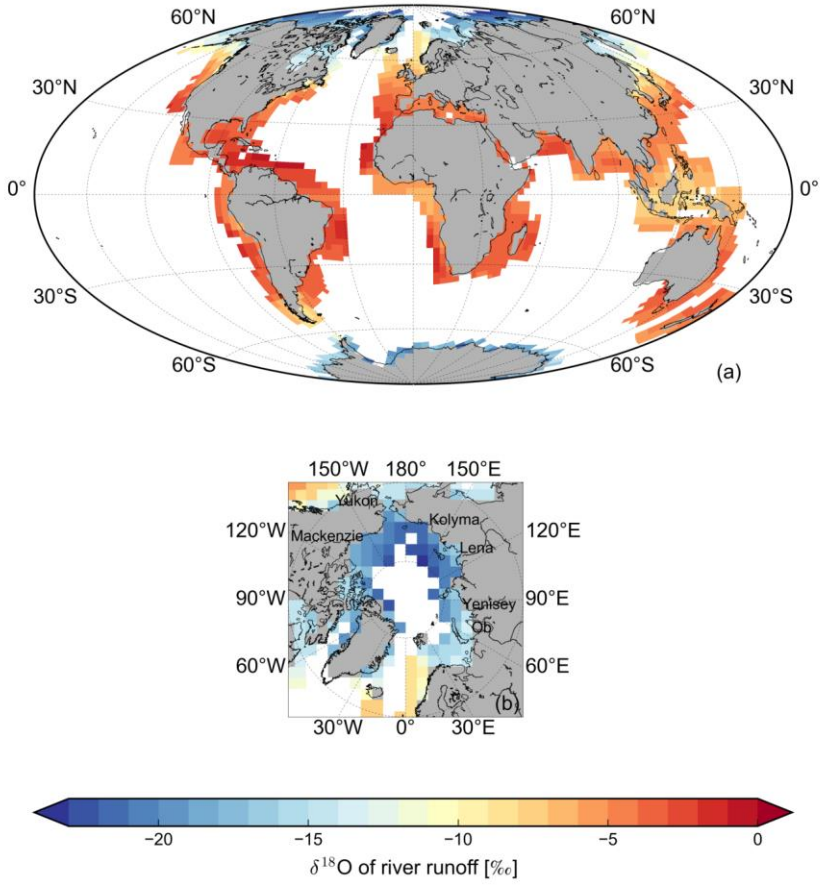

Figure 1329: Simulated annual mean $\delta^{18}O$ of river runoff in the upper 50 m for (a) the global ocean and (b) the Arctic Ocean with the approximate location of discharge of the six largest rivers.

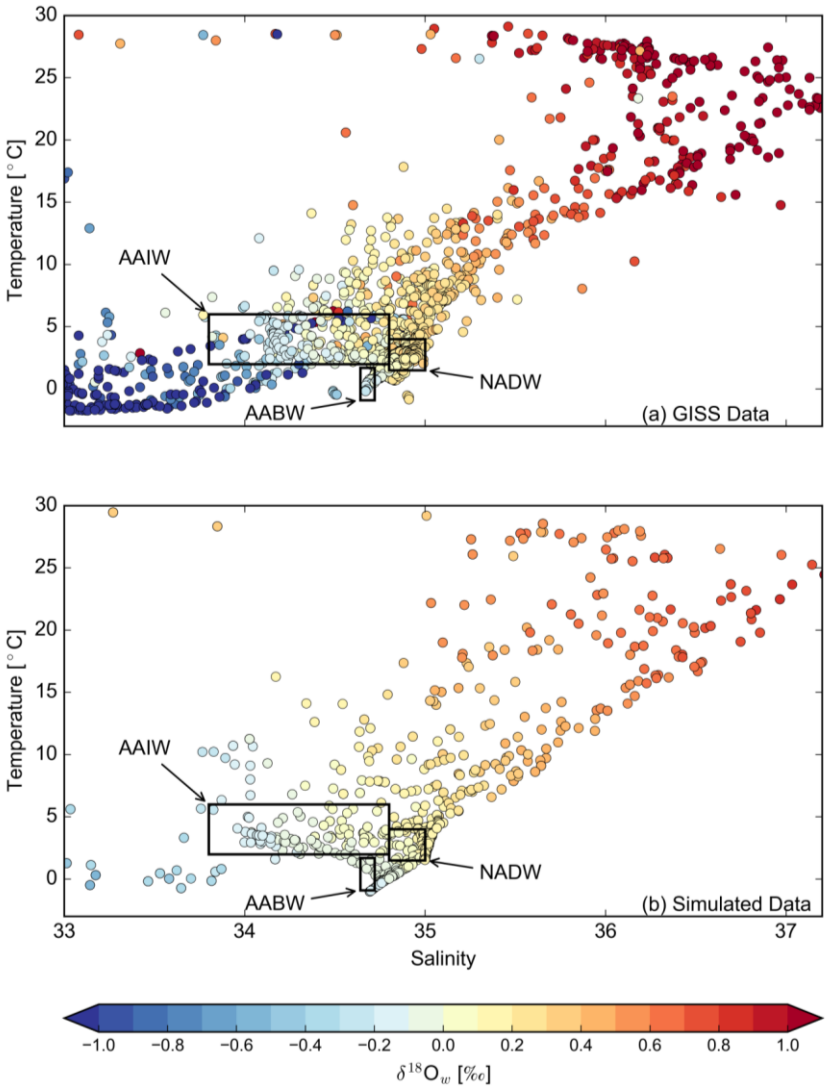
Temperature [° C]
AAIW
AABW
NADW
(a) GISS Data
(b) Simulated Data
Salinity
−1.0 −0.8 −0.6 −0.4 −0.2 0.0 0.2 0.4 0.6 0.8 1.0
$\delta^{18}O_w$ [‰]

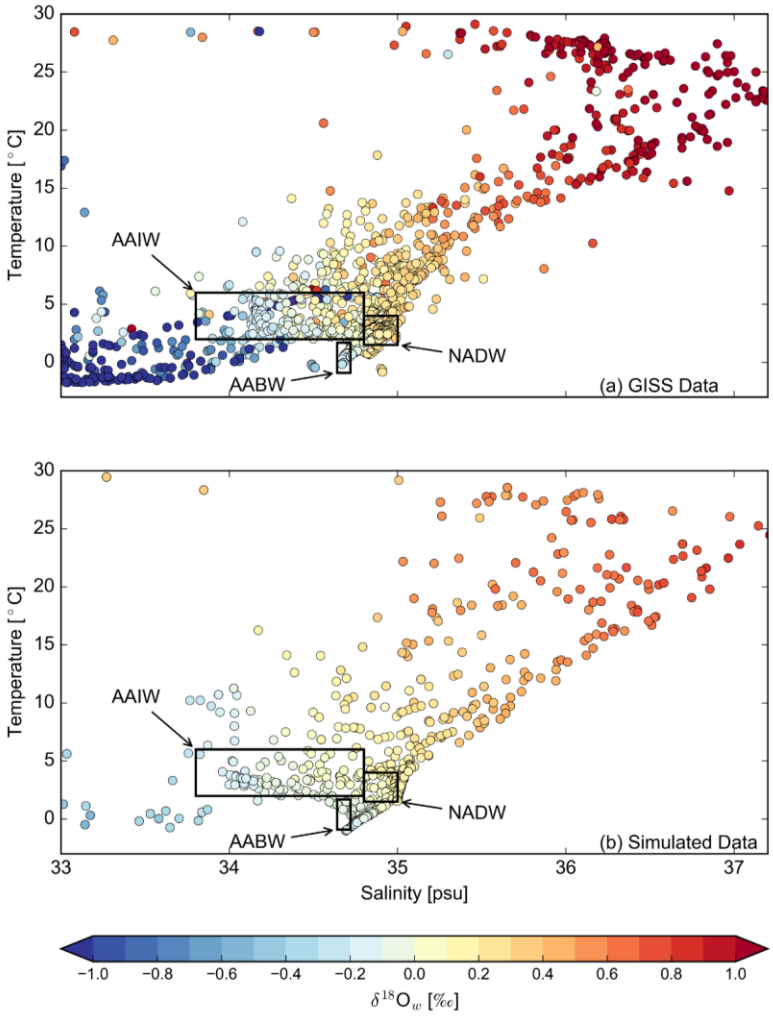

Figure 1430: Combined T-S-$\delta^{18}O_w$ diagrams for the (a) GISS data and (b) simulated data (annual mean) in the Atlantic Ocean. The temperature and salinity ranges for the different water masses in the Atlantic Ocean are defined according to Emery and Meincke (1986).

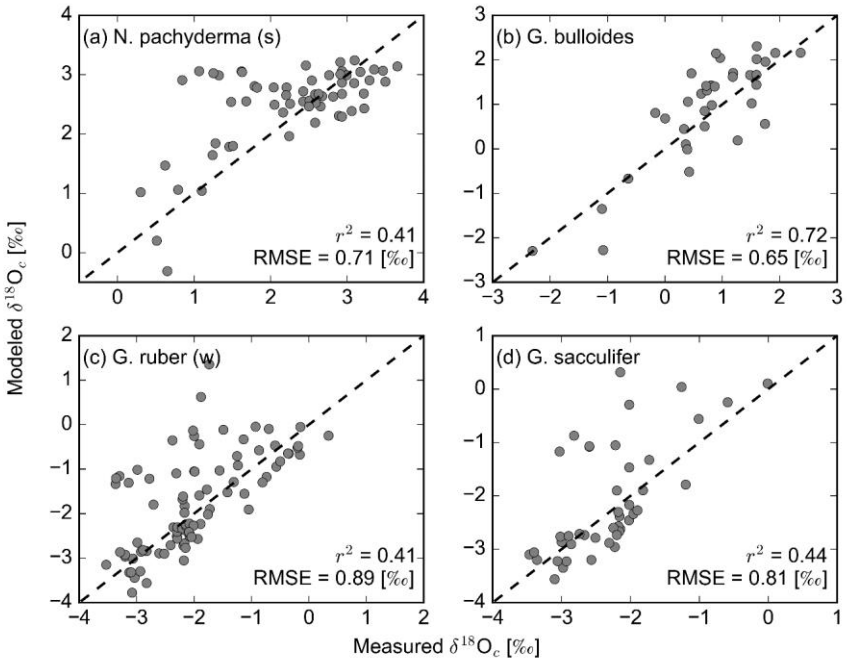

Figure 15: Relationship between measured $\delta^{18}O_c$ from plankton tow data (for references see text) and simulated long-term monthly mean $\delta^{18}O_c$ from the MITgcm for the individual species: (a) *N. pachyderma* (s), (b) *G. bulloides*, (c) *G. ruber* (w) and (d) *G. sacculifer*. For the comparison the specific month and depth of plankton tow sampling has been considered. Dashed lines represent the 1:1 line.

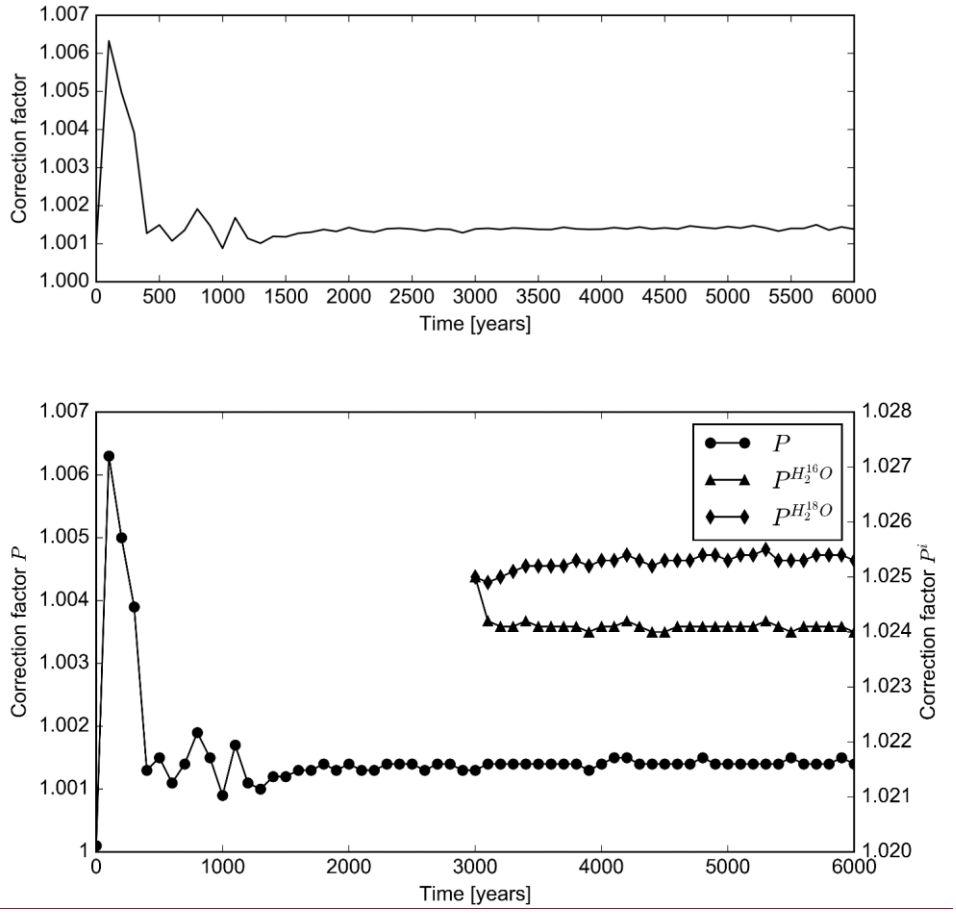

Figure A1: Time series of the ~~precipitation~~ correction factor for both, the precipitation and tracer specific precipitation throughout the model integration.